Title

An Analysis Of Simulated California Climate Using Multiple Dynamical And Statistical techniques

Authors

Miller, N. L.
Duffy, P. B.
Cayan, D. R.
et al.

Publication Date

2008-06-01

AN ANALYSIS OF SIMULATED CALIFORNIA CLIMATE USING MULTIPLE DYNAMICAL AND STATISTICAL TECHNIQUES

PIER PROJECT REPORT

Prepared For:
California Energy Commission
Public Interest Energy Research Program

Prepared By:
Lawrence Berkeley National Laboratory
Lawrence Livermore National Laboratory
University of California, Berkeley
University of California, San Diego
University of California, Santa Cruz
Utah State University, Logan
U.S. Geological Survey

June 2008
CEC-500-2008-XXX

California Climate Change Center
Report Series Number 2008-0XX

Prepared By:
N.L. Miller[1,2,*], P.B. Duffy[3], D.R. Cayan[4,5], H. Hidalgo[4], J. Jin[6,1], H. Kanamaru[4], M. Kanamitsu[4], T. O'Brien[7], N.J. Schlegel[2,1], L.C. Sloan[7], M.A. Snyder[7], K. Yoshimura[4]

[1]Lawrence Berkeley National Laboratory; [2]University of California, Berkeley; [3]Lawrence Livermore National Laboratory; [4]University of California, San Diego; [5]US Geological Survey; [6]Utah State University, [7]University of California, Santa Cruz,
* Corresponding Lead Author: NLMiller@LBL.gov

Commission Contract No. 500-XX-XXX
Commission Work Authorization No: MR-XX-XXX

Prepared For:
Public Interest Energy Research (PIER) Program
California Energy Commission

Guido Franco
Contract Manager

Kelly Birkinshaw
Program Area Lead
Energy-Related Environmental Research

Laurie ten Hope
Office Manager
Energy Systems Integration and Environmental Research Office

Martha Krebs
Deputy Director
ENERGY RESEARCH & DEVELOPMENT DIVISION

B.B. Blevins
Executive Director

Jackalyne Pfannenstiel
Chair

Acknowledgments

Support for this work was provided by the California Energy Commission PIER Program under the Climate Change Project. Work performed at Lawrence Berkeley National Laboratory and Lawrence Livermore National Laboratory is under the auspices of the U.S. Department of Energy under contract DE-AC03-76F00098 and W-7405-Eng-48, respectively. Model simulations performed by MK, HK, KY using *RSM*, MAS, TO'B, LCS using *RegCM*, JJ, NJS, NLM using *WRF-CLM* and *WRF-RUC*, and HH, DRC using *CANA*. We thank Peter Caldwell of LLNL for comments on the manuscript and NJS, JJ, PBD, and NLM for work on the report figures and analysis. Miller wrote the majority of this report and is the primary contact as lead author: nlmiller@lbl.gov.

Please cite this report as follows:

N.L. Miller, P.B. Duffy, D.R. Cayan, H. Hidalgo, J. Jin, H. Kanamaru, M. Kanamitsu, T. O'Brien, N.J. Schlegel, L.C. Sloan, M.A. Snyder, K. Yoshimura 2008. *An Evaluation of Simulated California Climate Using Multiple Dynamical and Statistical Downscaling Techniques.* The California Energy Commission, PIER Energy-Related Environmental Research Program. CEC-500-2008-XXX.

Preface

The Public Interest Energy Research (PIER) Program supports public interest energy research and development that will help improve the quality of life in California by bringing environmentally safe, affordable, and reliable energy services and products to the marketplace.

The PIER Program, managed by the California Energy Commission (Energy Commission), conducts public interest research, development, and demonstration (RD&D) projects to benefit California's electricity and natural gas ratepayers. The PIER Program strives to conduct the most promising public interest energy research by partnering with RD&D entities, including individuals, businesses, utilities, and public or private research institutions.

PIER funding efforts are focused on the following RD&D program areas:

- Buildings End-Use Energy Efficiency
- Energy-Related Environmental Research
- Energy Systems Integration
- Environmentally Preferred Advanced Generation
- Industrial/Agricultural/Water End-Use Energy Efficiency
- Renewable Energy Technologies
- Transportation

Drought analysis of the California Central Valley surface-groundwater-conveyance system is the final report for the project, Development and Application of a California Basin Water-Energy Model (contract number 500-02-004, work authorization number MR-05-05A) conducted by Lawrence Berkeley National Laboratory and the University of California, Berkeley in collaboration with the California DEpartment of Water Resources.

For more information on the PIER Program, please visit the Energy Commission's website www.energy.ca.gov/pier/ or contract the Energy Commission at (916) 654-5164.

Table of Contents

Figure 7a. Spatial mean Snow Water Equivalent (SWE) in a Sierra Nevada subdomain for WRF-CLM, WRF-RUC, RegCM3 with COOP observations. b: Simulated SWE in one high-elevation grid cell in RegCM3.

Figure 8. Taylor diagrams showing WRF-CLM, WRF-RUC, RSM, and RegCM model-to-observation performance scores based on normalized standard deviations and correlations for monthly means of (a) maximum temperature, (b) minimum temperature, (c) precipitation, and (d) SWE.

Figure 9. Surface latent heat fluxes. All results are climatological means for 1980-1989, for DJF (left two columns) and JJA (right two columns). Within each quadrant, the 4 panels show results from Regcm3, RSM, WRF-CLM, and the North American Regional Reanalysis (NARR). Top two rows show seasonal means from models and NARR; bottom two rows show differences between the models and NARR (i.e. model biases).

Figure 10. Same as Figure 9, except showing sensible hear flux at the surface.

Figure 11. Same as Figure 9, except showing downwelling solar radiation at the surface.

Figure. 12. Same as Figure 9, except showing vertically integrated cloud fraction. Results from WRF-CLM are not available.

Figure 13: Same as Figure 9, except showing upwelling solar radiation at the surface.

Figure 14: Same as Figure 9, except showing downwelling longwave radiation at the surface.

Figure 15: Same as Figure 9, except showing zonal wind component at the surface.

Figure 16: Same as Figure 9, except showing meridional wind component at the surface.

Figure 17. Geopotential Height (a) January mean-monthly distribution and (b) July mean-monthly distribution.

Figure 18. Model and Reanalysis comparison of the 500 hPa geopotential height for three locations P1. 120W, 39N (American River Basin), P2. 117.5W, 37N (Merced Basin), and P3. 122.5W, 38N (Russian River Basin).

Figure 19. Hovmueller plots of the 500 hPa geopotential heights (a) 38.5N and (b) 34N.

Figure 20. Hovmueller plots of the winter precipitation across latitude 38.5N.

Abstract

Four dynamic regional climate models (RCMs) and one statistical downscaling approach were used to downscale 10 years of historical climate in California. To isolate possible limitations of the downscaling methods, we used initial and lateral boundary conditions from the NCEP global reanalysis. Results of this downscaling were compared to observations and to an independent, fine-resolution reanalysis (NARR). This evaluation is preparation for simulations of future-climate scenarios, the second phase of this CEC scenarios project. Each model has its own strengths and weaknesses, which are reported here. In general, the dynamic models perform as well as other state-of-the-art dynamical regional climate models, and the statistical model has comparable or superior skill, although for a very limited set of meteorological variables. As is typical, the dynamical models have the most trouble simulating clouds, precipitation, and related processes, especially snow. This suggests that the weakest aspects of the models are parameterized subgrid scale processes, the hydrological cycle, and land surface processes. However, the resulting probabilistic ensemble simulations result in reduced model uncertainty and a better understanding of model spread.

Keyword: California climate, baseline simulation, dynamic and statistic downscaling

Executive Summary

Introduction

The Energy Commission Public Interest Energy Research (PIER) Program is developing probabilistic climate change scenarios for California. These scenarios will be used for both State planning and research activities. Recent PIER Reports (e.g. PIER Reports 2005-006, 2005-019) have indicated a need to (1) further enhance the performance of Regional Climate Models (RCMs) and (2) inter-compare RCMs, evaluating how well these models perform with such new enhancements when simulating California's climate. The RCM Enhancement and Baseline Climate Intercomparison (REBI) study presented here builds upon several earlier CEC-funded projects with a goal of quantifying and reducing RCM uncertainties, and comparing RCM 10 km resolution simulations of historical climate in California to observations, to each other, and to statistically downscaled simulations of climate. The current REBI-RACS project is the final phase of the REBI effort leading to the first phase of the RCM Analysis of Climate change Sensitivities (RACS), where each model is forced by IPCC global climate model outputs.

Purpose

The purpose of this study is to perform a series of numerical simulations, both dynamic and statistically based, to determine model performance limitations and to generate a baseline set of model climatologies as part of the scenarios projection preparations. The follow-on project, RACS, will rely on these results for better understanding model biases, signal-to-noise, and to reduce model uncertainties.

Project Objectives

The objectives are to develop California regional intercomparisons and bias analysis, and to complete the first phase of the sensitivity analysis of projected climate change in California at fine scale. This analysis is of high value to the climate science research community, impact assessment community, and California policy makers. The set of research RCMs have improved simulations with quantification of the reduced errors.

Project Outcomes

The output data from the NCAR/NCEP II Reanalysis-forced RCMs (WRF-CLM3, WRF-RUC, RegCM3, RSM) for the integration period 1980 – 1989 has been examined for model performance and skill. The specific analysis is based on MatLab analysis and plotting tools, and the PCMDI Climate Data Analysis Tool (CDAT), NCAR Command Language (NCL), and the AMWG Diagnostics Package.

Variables that have been analyzed include; total precipitation, maximum and minimum daily surface air temperature, surface specific humidity, surface downwelling shortwave radiation, zonal and meridional surface wind speed, snow depth, surface latent heat

flux, surface sensible heat flux, surface downwelling and upwelling longwave radiation, outgoing longwave radiation, and 500 hPa geopotential height.

Conclusions

Understanding the details of model errors and how each model has propagated such errors has further advanced our current probabilistic understanding of the potential consequences of climate change in California. The dynamically downscaled RCM sensitivity analysis provides the statistical downscaling procedures with a separate set of intercomparisons, and will provide the California impacts models with multiple variables in ensemble form.

1. Introduction

California's climate, hydrology, and ecology represent one of the most diverse and sensitive regional systems in the U.S., with over 1100 miles of coastline, desert regions, irrigated agricultural regions, and mountainous snowpack water storage regions. It has been determined in previous studies (IPCC 2001, 2007, USGCRP 2001, CA Ass 2001, 2006) that California's ecosystems, water resources, and infrastructure are at significant risk due to heat absorbing atmospheric greenhouse gasses (GHG) in the form of carbon dioxide from fossil fuels. In 2006 the California State Legislature passed, and the Governor signed into law, Assembly Bill 32 (AB32), the California Global Warming Solutions Act. AB32 establishes a "*first-in-the-world comprehensive program of regulatory and market mechanisms to achieve real, cost-effective reductions of greenhouse gasses (GHG).*" It makes the California Air Resources Board (CARB) responsible for monitoring and reducing GHG emission reduction targets in California to 2000 levels by 2010, and 1990 levels by 2020. AB32 requires the CARB to coordinate oversight of the efforts made to meet these targets and report to the Governor and the State Legislature biannually on progress made toward meeting the GHG emission reduction targets and climate change impacts to California. This includes impacts to water supply, public health, agriculture, the coastline, and forestry. As part of the biannual reporting process, a series of regional climate model simulations and analyses of present and projected climate are being prepared and used as input for a number of California impacts studies to meet the AB32 reporting requirement.

As an initial step towards fully quantifying the range of climate variability and change in California (CA) at high spatial resolution (10-km), one statistical and three dynamical downscaling approaches are intercompared and evaluated against observations. The rationale here is to test the usefulness and appropriateness of the different climate downscaling techniques based on observational data availability, computational constraints, climate stationarity assumptions, and model parameterizations. Each approach has uniquely different, and in some cases similar, advantages and disadvantages.

Climate model evaluation and intercomparison provides quantitative evaluations of model and process performance using observations and other models as standards for comparison. It allows for model advancements, leading to reduced errors and improved model performance. Climate model intercomparisons are essential for understanding how model-simulated projections of the future compare with the present. Improved model performance will allow for better decision making of actions needed for climate change mitigation, adaptation, and coping strategies.

Since 1989, the DOE'S Program for Climate Model Diagnostics and Intercomparison (PCMDI) has led the intercomparison of global-scale general circulation models (GCMs). The PCMDI mission is to develop and apply improved methods and tools for the diagnosis and intercomparison of GCMs, and represents a quality control gatekeeper for the GCMs that are part of the Intergovernmental Panel on Climate

Change (IPCC). While GCMs provide an important understanding of the climate on subcontinental and larger scales, they are unable to resolve fine-scale climate features and forcings that are of importance at local-to-regional scales; hence downscaling techniques have and will continue to be an essential element of climate change impacts analysis.

Dynamical downscaling uses a fine-resolution climate model having a global or smaller domain to produce fine-scale information. Physical knowledge comes from laws describing the atmosphere included in the fine-resolution model. If it has a limited geographical domain, this model is driven by initial and boundary conditions from a coarse simulation with a larger (typically global) domain. Required boundary condition data for limited-domain model includes 3-dimensional atmospheric fields at 3-hour or 6-hour intervals; this involves a large data volume, and few climate simulations save this output. Thus, most coarse-resolution climate simulations cannot be downscaling using a nested, limited-domain model. This restriction has recently been studied in detail by Yoshimura and Kanamitsu 2008, who proposed a method to relax this restriction. Global high-resolution simulations can be performed using only monthly-mean sea-surface temperatures and sea ice concentrations as boundary data; this is available from virtually all simulations. Thus this technique is widely applicable; an additional advantage is that it provides global downscaled data. It is, however, much more computationally demanding than using a limited-domain model. Dynamical downscaling in general is computationally demanding, but produces a complete range of physically consistent meteorological output. Because of this physical consistency, the output is useful for research on physical mechanisms of the local scale climate change. The most important shortcoming of dynamical downscaling is errors in the dynamical models (both nested and large-scale). Many of the model errors are systematic, but can be removed by using the differences or anomalies. This approach is frequently used in the study of changes due to global warming. .

Statistical downscaling uses empirical, data-driven techniques to produce fine-scale climate information. In the *constructed analogues* approach, relationships between local- or regional-scale climate features and large-scale features are developed by analyzing observations. Key assumptions in this approach are that the future climate patterns can be derived from linear combinations of the weather from a library of previously observed patterns, and that climate changes predicted using coarse-resolution models are correct at fine spatial scales. In another method, the delta change or perturbation approach, changes in key climate quantities (such as predicted temperature increases) from a coarse simulation are added (multiplied) to fine-scale historical climate data, producing a fine-scale future temperature (precipitation) prediction. An advantage is that using predicted *changes* from climate models results in a first-order elimination of biases from these models. Some analogue approaches also include bias correction (e.g. Imbert and Benestad, 2005). Statistical downscaling is computationally inexpensive, but in general produces results for only a few meteorological quantities (e.g. precipitation and near-surface temperatures). Another disadvantage of statistical downscaling is the difficulty of uncovering physical mechanisms behind unexpected results.

An important difference between dynamical and statistical approaches is that the latter, being empirical, do not require knowledge or accurate characterization of specific climate forcings; poor knowledge of these forcings (e.g. aerosols and land-use effects) can limit the fidelity of dynamically based simulations. This can be a disadvantage, however, if forcings change significantly between the period used for development/calibration of the statistical model and the period being simulated; this in general will result in violation of the stationarity assumption fundamental to statistical approaches.

In 2003, the California Energy Commission (CEC) sponsored a series of road-mapping exercises, including the report, *Modeling Regional Climate Change in California* (Gates, 2003). This report recommended the design of a regional climate model intercomparison protocol, control climate simulations, an evaluation and analysis of downscaling methods, development of a California database, and the development of a database access system. The present study builds upon the report recommendations, two previous CA investigations to intercompare climate model physics and dynamics (e.g. Duffy et al. 2006, Kueppers et al. 2008), and several past and ongoing regional climate investigations, such as the Program to Intercompare Regional Climate Simulations (PIRCS, Gutowski et al. 1998, 2000; Tackle et al. 1999), the North American Regional Climate Change Assessment Project (NARCCAP: Mearns et al. 2004), an Asian domain intercomparison (Leung et al. 1999; Fu et al. 2005), an Arctic RCM intercomparison (Curry and Lynch 2002), and a European intercomparison (PRUDENCE: Christensen et al. 2007; Déqué et al. 2007; Jacob et al. 2007).

The next section provides details of the approach for intercomparing and evaluating downscaled CA regional climate and model imitations. This is followed by an analysis of the results, significance, and applicability of each model with regard to AB32, and lastly a discussion with concluding summary.

2. Approach

The downscaling evaluation here includes one statistical and three dynamic approaches. In order to best evaluate the multi-model performance, domains, grids, and forcings were specified to be the same or as similar as possible. Each RCM used similar double nested domains and resolutions (Figure 1) with the same set of lateral boundary conditions and similar forcings, to generate 10-year baseline simulations for 1 January 1980 to 31 December 1989 at 30-km (outer nest) and 10-km (inner nest) resolutions. An exception is the RSM, which downscaled directly from 200 km resolution global reanalysis to 10 km resolution. Each model output includes a common set of variables and fluxes, mapped onto identical grids for analysis. This procedure follows the PCMDI protocols used for the IPCC AR4 intercomparisons. The statistical methods used the same inner domain as shown in Figure 1, but produced only precipitation and temperature fields at daily to monthly time-steps. In the following

subsection dynamic and statistical methods used in this study are discussed, followed by a subsection on the input data.

2.1 Dynamic and Statistical Downscaling

The Weather, Research, and Forecasting (WRF) model was developed at the National Center for Atmospheric Research (NCAR) and has been enhanced by LBNL researchers to include the NCAR Community Land Model version 3 (CLM3: Oleson et al. 2004), an advanced land surface scheme with sub-grid representation for advanced snow processes and dynamic vegetation with plant functional types, and lateral hydrologic flow capability. This enhancement to WRF, especially the subgrid representation and advanced snow processes, results significant error reductions (Section 3). The enhanced code, WRF-CLM, is set up with the Kain-Fritsch convection parameterization for cumulus clouds (Kain and Fritsch 1993), the Yonsei University (YSU) planetary boundary layer (PBL) scheme, and the Medium Range Forecast Model scheme (Hong and Pan 1996). The microphysics scheme used here is the WRF Single-Moment 3-class (WSM3) scheme (Hong et al. 2004). The Rapid Radiative Transfer Model (RRTM) is based on Mlawer et al. (1997) and is used for describing longwave radiation transfer within the atmosphere and to the surface; the shortwave radiation scheme was developed by Dudhia (1989).

The Regional Spectral Model (RSM; Juang and Kanamitsu 1994) originates from the one used at the National Centers for Environmental Prediction (NCEP), but the code was updated with greater flexibility and much higher efficiency (Kanamitsu et al. 2005) at the Scripps Institution of Oceanography. The RSM utilizes a spectral method (with sine and cosine series) in two dimensions. A unique aspect of the model is that the spectral decomposition is applied to the difference between the full field and the time-evolving background global analysis field. The model configuration and the downscaling methods are basically the same as that of CaRD10 (10 km California Reanalysis Downscaling; Kanamitsu and Kanamaru 2007), applying the scale-selective bias correction (SSBC, Kanamaru and Kanamitsu 2007) nudging scheme to the Reanalysis large-scale thermodynamic fields for a 10 km resolution simulation. Major updates from the CaRD10 project are: 1) Noah land surface model (Ek et al., 2003) with 4 soil layers instead of the 2-layered OSU (Pan and Mahrt 1987), 2) incorporation of cloud water and cloudiness as prognostic variables (Tiedtke 1993, Iacobellis and Sommerville, 2000) for better precipitation prediction, 3) a larger domain size: 19.506°–50.193°N, 135.314°–103.587°W, which are 180% and 175% larger in zonal and meridional directions than those of the CaRD10, to improve summer time monsoon flow from the Gulf of California, and 4) narrower lateral boundary nudging zones that extend only 2.5% of the total width in each of four lateral boundaries instead of 11.5% in CaRD10 to increase the useable domain.

The International Center for Theoretical Physics (ICTP) Regional Climate Model, RegCM3 (Pal et al., 2007), is a third-generation regional-scale climate model derived from the National Center for Atmospheric Research-Pennsylvania State (NCAR-PSU)

MM5 mesoscale model. RegCM3 uses the same dynamical core as MM5. RegCM3 also includes the Biosphere-Atmosphere Transfer Scheme (BATS1E: Dickinson et al., 1993) for surface process representation and the CCM3 radiative transfer package (Kiehl et al., 1996). RegCM3 documentation and source code are available at the ICTP, Trieste, Italy site; www.ictp.trieste.it/RegCNET/model.html. In this experiment, RegCM3 was configured with the Grell cumulus scheme (Grell, 1993) utilizing the Fritsch and Chappell closure scheme (Fritsch and Chappell, 1980) and the Holtslag boundary layer scheme (Holtslag and Boville, 1993). This version of BATS has 22 land-cover types and 3 soil layers, with rooting depth and other soil properties linked to land cover type.

The Constructed Analogues (CANA) statistical downscaling approach is based on the methods developed by van den Dool (2003) and has been presented by Hidalgo et al. (2008). The CANA method is based on the matching of daily Reanalysis weather patterns (e.g. precipitation and temperature) with previously observed weather patterns contained in an independent "library" of matching pairs of coarse-scale (Reanalysis) and corresponding high-resolution 1/8 degree (12-km) weather patterns (Maurer et al. 2002 data) for the same day. The 30 most similar historical patterns (analogues) to the Reanalysis pattern to be downscaled are used in a linear regression to produce a coarse-scale estimate for each day. The regression coefficients obtained from the coarse-scale analysis for each day are then applied to the corresponding 30 high-resolution analogue weather patterns to produce daily-downscaled estimates at 1/8 degree (Hidalgo et al. 2008). In this way, a large fraction of the daily variability of the weather patterns at high resolution is conserved. A comparison of the CANA method with the statistical method of bias correction following with spatial downscaling (Wood et al. 2004) can be found in Maurer and Hidalgo (2008). For the REBI analysis the library of previously observed patterns was selected from the period 1950 to 1978 so the downscaling period (1979-1999) is independent of the library used to derive the analogues.

In Hidalgo et al. (2008), the linear predictor equations were trained and validated for the period 1950 to 1999, where the even-numbered years were used for model calibration and odd-number years were used for model cross-validation. The CANA method showed very good skill (day to day validation correlations of the downscaled estimates with the observed data on the order of 0.7 or more) in downscaling coarse-scale temperature to a 12-km grid, and in reproducing precipitation in the coastal states of the western US, with less skill in the interior regions (Hidalgo et al. 2008).

2.2 Input Data

The National Centers for Environmental Prediction-Department of Energy Atmospheric Model Intercomparison Project II Reanalysis (NCEP/DOE-2) data were used for the dynamic model initial and lateral boundary conditions, as well as for training and validation of the CANA statistical model. The Sea Surface Temperatures (SSTs) were initialized with Atmospheric Model Intercomparison Project (AMIP) dataset for WRF and RegCM, while the European Reanalysis 40 year SST data (ERA40

http://www.ecmwf.int/research/era/do/get/era-40) was used for the RSM lower boundary conditions over the Pacific Ocean.

Model results are evaluated with the Parameter-elevation Regressions on Independent Slopes Model (PRISM) climatologies for California temperature and precipitation with monthly, yearly, and event-based climatic parameters (Daly et al. 2001, 2008). PRISM is a unique knowledge-based system. It includes point observations, digital grid estimates, digital elevation maps, and expert knowledge of climatic extremes, including rain shadows, coastal effects, and temperature inversions. The resulting PRISM climatologies are often taken as near-truth data sets and are used for numerous applications, including impacts analysis. Other simulated quantities are evaluated against the North American Regional Reanalysis (NARR; http://www.emc.ncep.noaa.gov/mmb/rreanl/) dataset. This is a fine-resolution reanalysis data product based on the Eta limited-domain model. Noteworthy features of NARR include direct assimilation of precipitation and some radiative fluxes. We use NARR to compare simulated quantities such as radiative fluxes for which adequate observations are not available.

Results of all REBI simulations were converted to a common format that adheres to standards developed for the climate and weather forecast (CF) community. The *CF conventions* specify standard variable names, dimension names, coordinate systems, calendars, metadata, etc. (http://cf-pcmdi.llnl.gov/documents/cf-conventions/1.0/cf-conventions.html) REBI model outputs were interpolated in the vertical to a standard set of atmospheric pressure levels. For certain analyses, such as calculating inter-model differences, results were interpolated to a common latitude/longitude grid having approximately the same 10-km grid spacing as the original RCM coordinate grids (1/12 degree in latitude and longitude).

3. Results

3.1 Climatological Means of Temperature and Precipitation

Three dynamic downscaling models (RegCM, RSM, WRF-CLM3), one statistical downscaling method (CANA), and a commonly-used, off-the-shelf, version of WRF (WRF-RUC), are evaluated and intercompared for model skill, as forced with the NCAR/NCEP Reanalysis II fields for 1980-1989. The climatological 10-year mean maximum and minimum 2-m air temperature and cumulative precipitation are shown for the winter and summer periods in Figures 2-6.

Figures 2a and b show spatial maps of California 10-year climatologies for June-August (JJA) daily maximum and minimum 2-m air temperature (T_{max}, T_{min}), respectively. Figure 3a and b shows their corresponding difference plots, as compared with the PRISM climatologies. The JJA maximum temperatures are well represented, with all models reproducing the large-scale spatial pattern of observed temperatures within the study domain. Nonetheless, all models have significant local biases. CANA and WRF-CLM shows cold biases along coastal regions. RSM is too warm (by 3-5^{o}C)

throughout the Central Valley, south coast, and Sierra. WRF-CLM3 has a strong cold bias in part of the Sierras, consistent with the existence of year-round snow (discussed below) in that region. RegCM3 shows overestimates near the coasts and in the south (i.e. 3-7^{o}C) over a smaller area than WRF-CLM, but is too cold in the Central Valley. This last issue is probably a result of a simplified representation of irrigation, in which surface soil moisture is fixed at 75% of field capacity. As noted below, this results in excessive latent heat fluxes, and hence a local cold bias. WRF-RUC shows larger JJA T_{max} overprediction for the Central Valley than WRF-CLM3. Similarly, the JJA minimum 2-m air temperature shows that the CANA performs well, with very slight underestimates along a north-south inland region, RSM has overestimates near the coast and southern inland region, with some overestimates in the southern foothills and mountains, WRF-CLM3 appears to have topographic over- and under-estimates, with significant overestimates in the inland south similar to RSM, WRF-RUC is generally too warm, and RegCM has topographic over- and under estimates, but somewhat less severe than WRF-CLM3. Comparison of results of WRF-RUC and WRF-CLM to those of the other models shows that simulated near-surface temperatures are roughly as sensitive to the land-surface scheme as other aspects of the model.

The winter December-February (DJF) maximum and minimum 2-m air temperatures (Figs. 4 and 5) behave quite similarly to the JJA , revealing slight overestimates for T_{max} in all cases, especially WRF-RUC and RSM in the Central Valley region. The DJF T_{min} differences show that CANA tends to have negative biases, whereas all the dynamical models (especially WRF-RUC) are largely too warm. The new coupling of CLM3 to WRF shows a dramatic reduction in this overestimate of T_{min}, but both WRF-CLM3 and RegCM are still too warm for DJF.

These differences in near surface temperature likely involve differences in land surface treatments (CLM-3, Noah and BATS) used in the three regional climate models. Full understanding of the temperature difference would require understanding effects of differences in specified land characteristics (vegetation type, surface roughness, albedo and soil type), as well as radiation fluxes and near surface meteorological parameters.

The cumulative November to March (NDJFM) precipitation and difference, as compared with the PRISM NDJFM precipitation climatologies are shown in figures 6a and b, respectively. Considerable effort was put into the evaluation and enhancement of models to optimize convective schemes (Shimpo and Kanamitsu, 2008) and to evaluate the SST sensitivity (Jin et al. 2008). All the models capture the large-scale spatial distribution of precipitation, which is dictated primarily by lateral boundary data and by topographic variations. However, the models exhibit significant biases in precipitation amounts: RegCM3, WRF-RUC, and to a lesser extent RSM are too wet in Sierra Nevada Mountains and in the wet Northwest part of the State. The difference plots show that CANA has smaller precipitation biases than any of the dynamical models, while WRF-CLM has the smallest biases among the dynamical models. WRF-RUC and RegCM3 are too wet everywhere in the State except the dry Southwest region. As noted below, RegCM3 seems to have insufficient latent heat fluxes over

ocean, particularly off the coast of Northern California. This makes the model's wet bias more remarkable, since not only is the correct amount of moisture entering the model domain, but also ocean evaporation is contributing too little to the water available for precipitation.

Overestimation of precipitation in an area of large precipitation is a common problem in high-resolution regional models, and is evident in three out of the four models analyzed here. (Nonetheless, PRISM may not be accurate over high topography areas.). The smaller bias in WRF-CLM3 likely results from use of the Kain and Fritsch parameterization scheme used in WRF-CLM3. A similar reduction in bias was observed in RSM test runs using Kain and Fritsch, but the high computer cost of this parameterization prevented its use in this study.

Model-based cumulative monthly precipitation is correlated in time with the PRISM precipitation in Figure 6c. The statistically downscaled CANA precipitation has excellent correlation with PRISM for most of the R field at or above 90%. The dynamic models cannot reach such high levels of correlation, however, RegCM3 does perform excellently (R > 90 percent) in the far northwest, while RSM is between 40 and 70 percent correlation, with its highest values showing up in the southern Sierra Nevada region. WRF-RUC has somewhat higher correlation values over a larger spatial domain and is an improvement over WRF-RUC.

3.2 Snow Water Equivalent

Accurate simulation of snow is important for studies of water resource and other societal impacts. Snow is a particularly difficult quantity to simulate, however, since it is sensitive to both meteorology (temperature and precipitation) as well as land surface processes. Furthermore, even if the atmospheric and land surface model physics is correct, snow in California will tend to be under-simulated as a result of finite model resolution; this results in truncated elevations in the mountains, and hence overly high surface temperatures. Our results, described below, exemplify the difficulty of accurately simulating snow cover in California.

Figure 7a shows Snow Water Equivalent (SWE) as a function of time for the 1980-1989 integration, using WRF-CLM3, WRF-RUC, RegCM3, and COOP observations (www.weather.gov/os/coop/coopmod.htm) over a Sierra Nevada sub-domain. (SWE results from RSM are discussed below, and CANA does not predict SWE). Alone among the models, WRF-CLM does a good job of simulating winter snow amounts, including year-to-year variability. As a result of this, its correlation coefficient against observed snow amounts (R=0.84) is higher than that of the other models. (R=0.61 for RegCM3 and R=0.50 for WRF-RUC). WRF-CLM's cold bias in night-time DJF temperatures in the Sierra (Figure 4b) probably does not affect simulated snow amounts, since even observed night-time temperatures in this season and region are below freezing. It is striking that WRF-RUC and RegCM3 underestimate winter snow despite over-estimating winter precipitation. On the other hand, WRF-CLM, and, to a lesser extent, RegCM3 erroneously preserve some snow cover throughout the year, even though RegCM3 significantly underestimates winter SWE. Figure 7b shows that

in some high-elevation grid cells in RegCM3 snow not only remains during the summer, but actually accumulates from year to year.

Other recent RCM evaluations (e.g. Leung and Qian, 2003, Duffy et al. 2006) have attributed a significant fraction of errors in simulated SWE to deficiencies in land-surface models (as opposed to meteorology). Slater et al. (2001) demonstrated the sensitivity of simulated SWE to land surface treatments, by forcing 18 off-line land-surface models with observed meteorology. In our simulations, WRF-CLM has a strong cold bias in JJA daily maximum temperatures in the Sierra Nevada Mountains. Thus the erroneous persistence of snow in this simulation could be a consequence of meteorological biases (although the presence of snow will amplify a cold bias). On the other hand, RegCM3 does not have a spatially consistent bias in maximum JJA temperatures in the Sierra. Hence in this simulation the summertime snow is likely due to a land-surface problem.

The RSM model simulated near-zero SWE at SNOTEL locations throughout the study period. One reason is that two SNOTEL stations are located on “water” grid cells in RSM (Lake Tahoe) where no snow is simulated. In addition, the RSM has a warm bias in near-surface temperatures on the lee side of the Sierra Nevada Mountains, and most of the precipitation there falls as a rain. Precipitation is also underestimated on the lee side. The SNOTEL stations compared in this paper are located near Lake Tahoe, which happens to be the area where the ratio of snowfall to precipitation decreases to a very low value in RSM. Also, most of SNOTEL stations are on leeward of the Sierras (at least in RSM topography), so there is very little snowfall in RSM. The SWE over the windward side and higher elevation seems to be a little more reasonable in RSM. The model precipitation and snowfall is very sensitive to small changes in topography and elevation in this area and care should be taken to select representative locations for evaluation of simulated SWE.

3.3 Spatio-temporal variability

Looking beyond biases in seasonal mean quantities, Taylor diagrams (Taylor, 2001) provide a convenient means to display pattern correlations and RMS errors between simulated and observed quantities, as well as a simple evaluation of the spatiotemporal variability of simulated quantities. Figure 8 shows Taylor diagrams of near-surface temperature, precipitation and SWE in our simulations. These are based upon monthly-mean quantities, mapped to a common spatial grid. The angular coordinate is the correlation coefficient between simulated and observed quantities, based upon monthly mean results at each grid cell. This evaluates if maxima and minima in the simulations occur at the correct times and geographical locations, but is independent of any errors in the magnitude of spatiotemporal variability. The latter is evaluated by the radial coordinate, which is the standard deviation of the models results for each month and grid cell, normalized by the same quantity in observations. (Again, this is calculated from monthly mean quantities at each grid cell, and thus reflects combined space and time variability.) The added value of a Taylor diagram is that the distance on the plot from the point marked “REF” on the horizontal axis is a normalized root mean square

(RMS) error; thus the Taylor diagram displays three useful statistical measures on a two-dimensional plot. All these measures are independent of errors in the mean (i.e., biases), so the Taylor diagrams complement information presented so far.

The Taylor diagrams show that all the simulations do well at representing spatiotemporal variability in daily minimum and (especially) daily maximum near-surface temperatures; the CANA results come close to matching the best of the dynamical models (RSM) in this respect. For precipitation, CANA again performs better than all the dynamical models except the RSM, despite seriously underestimating spatiotemporal variability. The excessive spatiotemporal variability of precipitation in RegCM3 and WRF-RUC seen in the Taylor diagram is due at least in part to these models' excessive precipitation in Northwest California and the Sierra Nevada mountains (Figure 6a).

RegCM3 and WRF-RUC in particular underestimate the spatiotemporal standard deviation of SWE; this is consistent with these models having far too little SWE in winter (Figure 7).

3.4 Surface Energy Fluxes and Clouds

In general, apparent biases in simulated surface energy fluxes can reflect deficiencies either in the models being evaluated or in NARR, which we use as a standard for comparison. (Of course apparent biases can always results from errors in the observational standard; we emphasize the possibility here since NARR is a model-based data product.). In some cases, as noted below, inter-model differences are at least as large as the differences between individual models and NARR; this implies significant biases in at least some of the models, regardless of any possible errors in NARR. Furthermore, in some cases noted below, biases in simulated surface energy fluxes clearly result from deficiencies in other aspects of the simulation.

As with other aspects of simulated climate, biases in surface energy fluxes can reflect errors in imposed climate forcings, as distinct from a model's representation of physical processes. For example, RegCM3 shows much higher latent heat fluxes in the Central Valley in JJA than NARR (and the other models). This results from enhanced soil moisture in RegCM3, which is imposed as a way of representing the climatic effects of large-scale irrigation. (Soil moisture content was constrained to be 75% of field capacity in irrigated regions and seasons.) This simple representation of irrigation also influences JJA sensible heat fluxes in RegCM3 (Figure 10). More generally, biases in simulated seasonal-mean latent heat fluxes (Figure 9) appear to correlate with biases in the seasonal mean of daily maximum temperatures. (Compare, e.g. Figure 3a to Figure 9).

The increased latent heat flux just off the coast of Los Angeles during DJF is a reflection of Santa Ana events (Kanamitsu and Kanamaru, 2008); this is very clearly shown in RegCM3 and RSM (somewhat obscured in WRF), but is not found in NARR. This is due to the coarse resolution (32km) used in NARR. The WRF simulation tends

to have maximum evaporation just off the coast, which is very different from other models.

NARR results for surface downwelling solar fluxes exhibit the expected large-scale features: fluxes are higher in summer than winter, in winter are lower in the Northern part of the State, and in summer are lower over the ocean (Figure 11). The biases in WRF-CLM and RSM in downwelling solar radiation (Figure 11) are consistent with their biases in vertically-integrated cloud fraction (Figure 12). The RSM model captures NARR's large-scale pattern of downwelling solar fluxes well in both seasons. All the models have relatively small biases in downwelling solar fluxes over land in summer, indicating that they are doing an adequate job of simulating the relatively little cloud cover in that season and region. Over ocean, however, WRF has too little downwelling solar, and RegCM3 has too much. In the case of RegCM3, we can verify that this reflects inadequate cloud cover (Figure 12). The largest cloud bias in RegCM3 is over Nevada, but the model's precipitation bias in largest in California. This presumably indicates reduced available moisture after air masses have passed over the California mountains. Over-land biases in downwelling solar are larger in winter; this is expected, since cloud cover, and hence potential for biases in cloud cover, are greater in winter. WRF-CLM's spatial pattern of downwelling solar flux is very different from that of the other models in both DJF and JJA. This presumably results from cloud biases, but this cannot be verified due to lack of availability of cloud results from WRF-CLM.

The largest local biases and apparent biases in upwelling solar fluxes (Figure 13) have to do with deficiencies in simulated snow cover. In DJF, all three models have much stronger solar radiation upwelling from the surface in the mountain regions than NARR does; this is largely a result of insufficient snow cover in NARR, due to its relatively coarse grid spacing (32 km). Hence this apparent model bias primarily reflects a limitation of NARR. On the other hand, both WRF-CLM and RegCM3 have a strong local maximum in upwelling solar in the mountains in summer (JJA). This is a consequence of these models having year-round snow in this region (discussed above), which is not observed.

Downwelling longwave radiation at the surface ("RLDS;" Figure 14a) reflects atmospheric temperature and moisture distributions as well as cloudiness distributions. RLDS is fairly similar among the models. The larger RLDS over ocean in WRF is consistent with its small downwelling short wave flux (Figure 11), and is presumably due to think clouds. Again RSM is very similar to NARR, but other models have clear positive biases, particularly over land.

3.5 Geopotential Heights and Surface Winds

The January and July 10-year climatological mean-monthly spatial plots of 500 mb geopotential height are shown in Figure 17. The January height fields show that all the models tend to be too high. For July, the spectral RSM replicates the large-scale Reanalysis forcing, while the RegCM3 underestimates height fields and the WRF appears to capture more detail associated with topographic disturbances. This is further

seen in Figure 18, where simulated mean-monthly geopotential heights are plotted against the NCEP/NCAR Reanalysis heights for three points, P1, 120W, 39N (American River Basin), P2, 117.5W, 37N (Merced Basin), and P3, 122.5W, 38N (Russian River Basin). A general conclusion that can be drawn from these results is that WRF underestimates geopotential heights, especially when the reanalysis heights are low.

To understand the time-evolution of the height fields, fields that reveal the presence of storm systems propagating through the study domain, Figure 19 provides model-reanalysis Hovmeuller plots of the mean-monthly 500 hPa geopotential heights for 1980 to 1989 for a northern California latitude (38.5N) and a southern California latitude (34.0N).

Except as noted below, the models reproduce the large-scale patterns in surface wind components estimated by NARR. Despite this, errors in individual grid cells can be comparable in magnitude to the wind component itself. In significant regions of Southern California, RegCM3 has an incorrect sign on one or both wind components.

As a further analysis of the model-simulated heights, we have added 1980 – 1989 precipitation Hovmeuller plots for Northern California and the Pacific Ocean at latitude 38.5 for longitudes -119 to -123, including the Russian and American River Basins. Figure 20 shows these results using PRISM, CANA, RSM, RegCM, WRF-CLM, and WRF-RUC. Precipitation making landfall is near -122 and shows good skill using CANA, WRF-CLM, and RSM, but is overestimated by RegCM, WRF-RUC. The American River Basin is closer to Longitude -123, where WRF-CLM shows the highest overall skill for this location.

4. Summary and Conclusions

Any downscaling approach is only as good as the large-scale forcing, and in this study we use reanalysis initial and boundary conditions to isolate shortcomings in the downscaling methods. To further isolate the effects of different model formulations, the three dynamic downscaling models (WRF-CLM, RegCM3, and RSM) that we ran and analyzed were configured with domains and grid spacing as close as possible to identical. Unique to each model are the parameterization schemes for boundary layer development, cloud physics, convection, and land surface processes. More important is the boundary condition updating method. The lateral boundary conditions differ most significantly between the spectral model (RSM) and the Cartesian models (RegCM3, WRF). Spectral updating is a fully internal procedure, where the large-scale values update the entire field, while latitude-longitude model updates are along a set of nudge points based on the Barnes (1973) or Cressman (1959) schemes. This difference is important for the way in which the internal dynamics sets up and the degree of independence the RCMs within the internal fields. Error propagation using the spectral approach may likely be more damped and when evaluating with the large-scale signals are better behaved.

As noted in detail above, all the models (dynamical and statistical) analyzed here have limitations. Nonetheless, they perform as well as other state-of-the-art downscaling systems, and all do a credible job simulating the historical climate of California. The empirically-based CANA statistical approach performs at least as well as the dynamical models; it is notably spatiotemporal variability of precipitation and near-surface temperature. Its errors tend to be distinct from those of the dynamical models. The most important limitation of this approach is the very limited set of output variables (near-surface temperature and precipitation) that have so far been predicted using this method. There is no fundamental reason why additional meteorological quantities could not be simulated sing this approach.

The dynamical models do better at simulating the large-scale circulation (as diagnosed by 500 mb heights), surface winds and near-surface temperatures than parameterized quantities such as clouds, precipitation, and snow cover. Errors in these quantities lead to errors in others; for example, deficiencies in cloud amounts and snow cover results in large errors on downwelling and upwelling short-wave fluxes. Snow cover is particularly difficult to simulate, being sensitive to both simulated meteorology and land surface processes. None of the models evaluated here simulated year-round snow cover well. Among the dynamical models, WRF-CLM performs best at simulating seasonal precipitation amounts.

5. Acknowledgements: This work was supported by the CEC PIER Program under the Climate Change Project. Work performed at Lawrence Berkeley National Laboratory and Lawrence Livermore National Laboratory is under the auspices of the U.S. Department of Energy under contract DE-AC03-76F00098 and W-7405-Eng-48, respectively. We thank Peter Caldwell of LLNL for comments on the manuscript.

6. References

Barnes, S.L., 1973: Mesoscale objective analysis using weighted time-series observations. NOAA Tech. Memo. ERL NSSL-62. National Severe Storms Laboratory, Norman, OK 73069, 60 pp. [NTIS COM-73-10781]

Benestad, R. E. 2004: Empirical-Statistical Downscaling in Climate Modeling, *EOS*, *85*, No.42, 19 October 2004.

Christensen, J.H., Carter, T.R., Rummukainen M., and Amanatidis, G. 2007. Evaluating the performance and utility of climate models: the PRUDENCE project. *Climatic Change, Vol 81*. doi:10.1007/s10584-006-9211-6.

Chou, M.D. and M. J. Suarez, 1994: An efficient thermal infrared radiation parameterization for use in General Circulation Models. Technical Report Series on Global Modeling and Data Assimilation, National Aeronautical and Space Administration/TM-1994-104606, 3, 85 pp.

Chou, M.D., and K.T. Lee, 1996: Parameterizations for the Absorption of Solar Radiation by Water Vapor and Ozone. J. Atmos. Sci., 53, 1203-1208.

Chou, M.-D., and M. J. Suarez, 1999: A shortwave radiation parameterization for atmospheric studies. NASA Tech. Memo. 15(104606), 40 pp.

Cressman, G.P., 1959: An operational objective analysis system. Month. Wea. Rev., 87, 367-374.

Curry, J.A., and A.H. Lynch, 2002: Comparing Arctic Regional Climate Models. *EOS*, *83*, 87.

Daly, C., G.H. Taylor, W. P. Gibson, T.W. Parzybok, G. L. Johnson, P. Pasteris. 2001. High-

quality spatial climate data sets for the United States and beyond. *Transactions of the American Society of Agricultural Engineers*, *43:* 1957-1962.

Daly, C., Halbleib, M., Smith, J.I., Gibson, W.P., Doggett, M.K., Taylor, G.H., Curtis, J., and Pasteris, P.A. 2008. Physiographically-sensitive mapping of temperature and precipitation across the conterminous United States. *International Journal of Climatology*, DOI: 10.1002/joc.1688.

Déqué, M., Rowell, D.P., Lüthi, D., Giorgi, F., Christensen, J.H., Rockel, B., Jacob, D., Kjellström, E., de Castro, M. and van den Hurk, B. 2007: An intercomparison of regional climate simulations for Europe: assessing uncertainties in model projections. *Climatic Change. 81.* doi:10007/s10584-006-9228-x.

Dickinson, R.E., Henderson-Sellers, A. and Kennedy, P.J., 1993. Biosphere-Atmosphere Transfer Scheme (BATS) Version 1e as Coupled to the NCAR Community Climate Model. NCAR TN-387+STR, NCAR, Boulder, CO.

Duffy, P.B., R.W. Arritt, J. Coquard, W. Gutowski, J. Han, J. Iorio, J. Kim, L.-R. Leung, J. Roads and E. Zeledon, 2006: Simulations of present and future climates in the western U.S. with four nested regional climate models. *J. Climate, 19*, 873-895.

Ek, M. B., K. E. Mitchell, Y. Lin, E. Rogers, P. Grunmann, V. Koren, G. Gayno, J. D. Tarpley, 2003: Implementation of Noah land surface model advances in the National Centers for Environmental Prediction operational mesoscale Eta model, *J. Geophys. Res.*, *108* (D22), 8851, doi:10.1029/2002JD003296.

Fritsch, J.M. and Chappell, C.F., 1980. Numerical Prediction of Convectively Driven Mesoscale Pressure Systems .1. Convective Parameterization. J*ournal of the Atmospheric Sciences, 37*(8): 1722-1733.

Fu, C. B., S. Y. Wang, Z. Xiong, W. J. Gutowski, D. K. Lee, J.McGregor, Y.Sato, H. Kato, J.-W. Kim, M.-S. Su, 2005: Regional Climate Model Intercomparison Project for Asia (RMIP). *Bull. Amer. Meteor. Soc*.

Gates, W.L., 2003: Modeling regional climate change in California. CEC Report P500-03-025FA1, 18pp.

Grell, G. A., 1993: Prognostic Evaluation of Assumptions Used by Cumulus Parameterizations. *Monthly Weather Review*, *121,* 764-787.

Grell, G.A. and D. Devenyi, 2002: A generalized approach to parameterizing convection combining ensemble and data assimilation techniques, *Geoph. Res. Let*., **29** (14), 10.1029/2002GL015311, 2002.

Gutowski, W. J., G. L. Potter and M. R. Riches, 1988: DOE model intercomparison workshop II. *Bull. Am. Meteor. Soc*., 69, 1453–1454.

Gutowski, W. J., E. S. Takle and R. W. Arritt, 1998: Project to Intercompare Regional Climate Simulations - Workshop II, 5 - 6 June 1997. *Bull. Am. Meteor. Soc*., *79*, 657-659.

Gutowski, W.J., R.W. Arritt, E., S. Takle, Z. Pan, F. Giorgi, J.H. Christensen, S.-Y. Hong, W. M. Lapenta, G.E. Liston, J. McGregor, and J.O. Roads, 2000: Project to Intercompare Regional Climate Simulations: Advancing the CLIVAR Agenda. CLIVAR Exchanges, 5, 13-15.

Hidalgo, H. G., M. D. Dettinger, and D. R. Cayan. 2008. *Downscaling with Constructed Analogues: Daily Precipitation and Temperature Fields Over the United States*. California Energy Commission, PIER Energy-Related Environmental Research. CEC-500-2007-123. 48 Pp. Available on-line: http://www.energy.ca.gov/2007publications/CEC-500-2007-123/CEC-500-2007-123.PDF.

Holtslag, A.A.M. and Boville, B.A., 1993. Local Versus Nonlocal Boundary-Layer Diffusion in a Global Climate Model. *Journal of Climate, 6*(10): 1825-1842.

Hong, S.Y., and H.L. Pan, 1996: Nonlocal Boundary Layer Vertical Diffusion in a Medium-Range Forecast Model. Mon. Wea. Rev., 124, 2322-2339.

Hong, S.-Y., J. Dudhia, and S.-H. Chen, 2004: A Revised Approach to Ice Microphysical Processes for the Bulk Parameterization of Clouds and Precipitation, Mon. Wea. Rev., 132, 103–120.

Iacobellis, S.F., and R.C.J. Somerville, 2000: Implications of Microphysics for Cloud-Radiation Parameterizations: Lessons from TOGA COARE. *J. Atmos. Sci.*, **57**, 161–183.

Imbert, A., and R. E. Benestad, 2005: An improvement of analog model strategy for more reliable local climate change scenarios, *Theoretical and Applied Climatology*, *82*, Numbers 3-4 / September, 2005, DOI 10.1007/s00704-005-0133-4.

Jacob, D., Bärring, L., Christensen, O.B., Christensen, J.H., de Castro, M., Déque, M., Giorgi, F., Hagemann, S., Hirschi, M., Jones, R., Kjellström, E., Lenderink, G., Rockel, B., Sánchez, E., Schär, C., Seneviratne, S.I., Somot, S., van Ulden A. and van den Hurk, B., 2007: An inter-comparison of regional climate models for Europe: Design of the experiments and model performance. *Climatic Change. Vol. 81.* doi:10007/s10584-006-9213-4.

Janjic, Z. I., 1996: The Mellor-Yamada level 2.5 scheme in the NCEP Eta Model. 11th Conference on Numerical Weather Prediction, Norfolk, VA, 19-23 August 1996; American Meteorological Society, Boston, MA, 333-334.

Jin, J., N.J. Schlegel, and N.L. Miller, 2008: Analysis of Sea Surface Temperature Boundary Conditions Using the Weather Research and Forecasting Model, Spring AGU Joint Assembly, Ft. Lauderdale, FL, 30 May 2008.

Juang, H.-M.H. and M. Kanamitsu, 1994: The NMC nested regional spectral model. *Mon. Wea. Rev.*, *122*, 3-26.

Kain, J.S., 2004: The Kain-Fritsch convective parameterization: An update. *J. Applied Meteor.*, **43**, 170-181.

Kanamitsu, M. and H. Kanamaru, 2007: 57-Year California Reanalysis Downscaling at 10km (CaRD10) Part 1. System Detail and Validation with Observations. *J. Climate, 20*, 5527-5552.

Kanamitsu, M., H. Kanamaru, Y. Cui and H. Juang. 2005: Parallel Implementation of the Regional Spectral Atmospheric Model. CEC-500-2005-014. Available from http://www.energy.ca.gov/2005publications/CEC-500-2005-014/CEC-500-2005-014.

Kanamaru, H. and M. Kanamitsu, 2007: Scale-Selective Bias Correction in a Downscaling of Global Analysis using a Regional Model. *Monthly Weather Review*, *135* (2), 334–350.

Kiehl, J.T. et al., 1996. Description of the NCAR Community Climate Model (CCM3). NCAR TN-420+STR, CGD, NCAR.

Kueppers, L.M., M.A. Synder, L.C. Sloan, D. Cayan, J. Jin, H. Kanamaru, M. Kanamitsu, N.L. Miller, M. Tyree, H. Du, and B. Weare, 2008: Regional climate effects of irrigation and urbanization in the western United States: A model intercomparison. *Global and Planetary Change 60*: 250–264.

Leung, L.R., S.J. Ghan, Z-C Zhao, Y. Luo, W-C Wang, W-L Wei, 1999: Intercomparison of regional climate simulations of the 1991 summer monsoon in eastern Asia. *J. Geophys. Res., 104*, 6425-6454.

Leung, L.R., and Y. Qian, 2003: The sensitivity of precipitation and snowpack simulations to model resolution via nesting in regions of complex terrain. *J. Hydrometeorol.*, 4, 1025-1043.

Lin, Y.-L., R. D. Farley, and H. D. Orville, 1983: Bulk parameterization of the snow field in a cloud model. *J. Climate Appl. Meteor.*, 22, 1065–1092.

Maurer, E.P. and H.G. Hidalgo, 2008: Utility of daily vs. monthly large-scale climate data: an intercomparison of two statistical downscaling methods. *Hydrology and Earth System Sciences.* 12, 551-563.

Mearns, L.: NARCCAP North American Regional Climate Change Assessment Program A Multiple AOGCM and RCM Climate Scenario Project over North America. 12/17/2004. AGU

Fall Meeting, San Fransisco, USA.

Miller, N.L., J. Kim, R.K. Hartman, and J.D. Farrara, 1999: Downscaled climate and streamflow study of the southwestern United States, *JAWRA* – Special Issue on Climate Change and Water Resources, *35*, 1525-1537.

Mlawer, E. J., S. J. Taubman, P. D. Brown, M. J. Iacono, and S. A. Clough, 1997: Radiative transfer for inhomogeneous atmosphere: RRTM, a validated correlated-k model for the long-wave. *J. Geophys. Res*., 102 (D14), 16663-16682.

Moorthi, S., and M. J. Suarez, 1992: Relaxed Arakawa-Schubert: A parameterization of moist convection for general circulation models. *Mon. Wea. Rev.,* **120,** 978-1002.

Pal, J.S., F. Giorgi, X. Bi, N. Elguindi, F. Solmon, X. Gao, R. Francisco, A. Zakey, J. Winter, M. Ashfaq, F. Syed, J.L. Bell, N.S. Diffenbaugh, J. Karmacharya, A. Konare, D. Martinez, R.P. da Rocha, L.C. Sloan and A. Steiner, 2005: The ICTP RegCM3 and RegCNET: Regional Climate Modeling for the Developing World, submitted to BAMS.

Pal, J. S. et al., 2007: Regional climate modeling for the developing world - The ICTP RegCM3 and RegCNET." *Bulletin of the American Meteorological Society 88*: 1395-

Pan, Z., J. H. Christensen, R.W. Arritt, W.J. Gutowski, Jr., E.S. Takle, and F. Otieno, 2001: Evaluation of uncertainties in regional climate change simulations. *J. Geophys. Res*., 106, 17,735-17,752.

Pan, H.-L. and L. Mahrt, 1987: Interaction between soil hydrology and boundary layer developments. *Boundary-Layer Meteor.*, *38,* 185-202.

Salathe E., 2002: Comparison of Various Precipitation Downscaling Methods for the Simulation of Streamflow in a Rainshadow River Basin. http://www.atmos.washington.edu/~salathe/papers/downscale/yakima.html

Slater, A.G., C. A. Schlosser, C. E. Desborough , A. J. Pitman, A. Henderson- Sellers , A. Robock , K. Ya. Vinnikov , K. Mitchell, A. Boone, H. Braden, F. Chen, P. Cox, P. de Rosnay, R.E. Dickinson, Y-J. Dai, Q. Duan, J. Entin, P. Etchevers, N. Gedney, Ye. M. Gusev, F. Habets, J.Kim, V. Koren, E.Kowalczyk, O.N.Nasonova, J.Noilhan, J. Shaake, A.B. Shmakin,T. Smirnova, D. Verseghy, P. Wetzel , Y. Xue, Z-L. Yang, 2001: The representation of snow in land-surface schemes: results from PILPS 2(d), *J. Hydrometeorology, 2*, pp. 7-25.

Shimpo, A. and M. Kanamitsu, 2008: Comparison of Four Cloud Schemes in Simulating the Seasonal Mean Field Forced by the Observed Sea Surface Temperature. In print, Mon. Wea. Rev.

Skamarock, W. C., J. B. Klemp, J. Dudhia, D. O. Gill, D. M. Barker, W. Wang and J. G. Powers, 2005: A Description of the Advanced Research WRF Version 2, NCAR Tech Note, NCAR/TN–468+STR, 88 pp.

Takle, E. S., W. J. Gutowski, R. A. Arritt, Z. Pan, C. J. Anderson, R. R. da Silva, D. Caya, S.-C. Chen, J. H. Christensen, S.-Y. Hong, H.-M. H. Juang, J. Katzfey, W. M. Lapenta, R. Laprise, P. Lopez, J. McGregor and J. O. Roads, 1999: Project to Intercompare Regional Climate Simulations (PIRCS): Description and initial results. . *J. Geophys. Res*., 104, 19,443-19,461.

Taylor, K. E., Summarizing multiple aspects of model performance in single diagram, *J. Geophys. Res., 106*, D7, 7183--7192, 2001.

Tiedtke, M., 1993: Representation of Clouds in Large-Scale Models. *Mon. Wea. Rev., 121*, 3040–3061.

Wilby R.L. and T.M.L. Wigley. 2000. Precipitation predictors for downscaling: Observed and general circulation model relationships. *International Journal of Climatology. 20*: 641-661.

Wood, A. W., L. R. Leung, V. Sridhar, and D. P. Lettenmaier. 2004. Hydrologic implications of dynamical and statistical approaches to downscaling climate model outputs, *Climatic Change, 62*, 189-216.

Zorita, E., and H. von Storch, 1999: The Analog Method as a Simple Statistical Downscaling Technique: Comparison with More Complicated Methods, *J. Climate, 12*, pp. 2474–2489. DOI: 10.1175/1520-0442(1999)012<2474:TAMAAS>2.0.CO;2.

7. Tables and Figures:

Table 1. Summary of RCM settings

	RegCM3	**RSM**	**WRF-CLM**	**WRF-RUC**
Land Surface	BATS1E Dickinson 1986	NOAH Mitchell et al. 2002	CLM3 Oleson et al. 2002	RUC
Microphysics	Orville and Kopp 1977	Iacobellis and Somerville 2003	Lin et al. 1983	WSM 3-class simple ice scheme (Hong et al. 2004)
Shortwave Radiation	Kiehl et al. 1996	Chou and Lee 1996	Goddard Chou and Suarez 1999	Goddard Chou and Suarez 1999
Longwave Radiation	Kiehl et al. 1996	Chou and Suarez 1994	RRTM Mlawer et al. 1997	RRTM Mlawer et al. 1997
Planetary Boundary	Holstag and Boville 1993	Hong and Pan 1996	Mellor-Yamada 1982	Mellor-Yamada 1982
Cumulus	Grell 1993	Moorthi and Suarez 1992	Grell-Devenyl 2002	Kain-Fritsch scheme Kain 2004

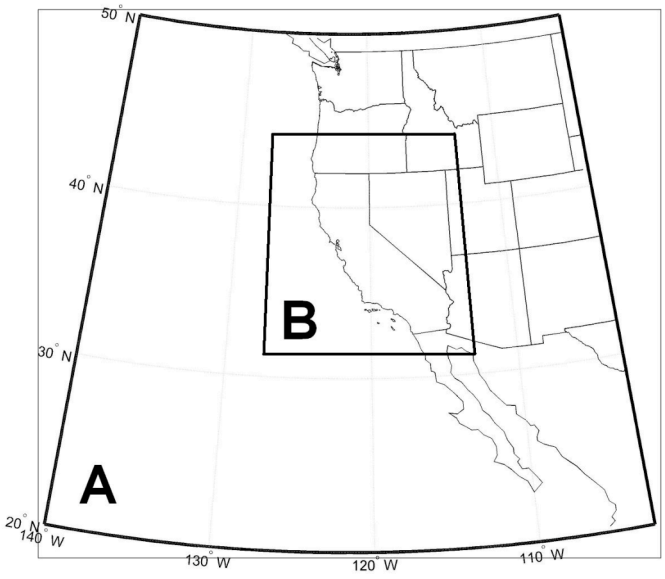

Figure 1. Model domains used in this study**.** A. Western U.S. and Eastern Pacific Ocean, 30-km resolution, [139W21N x 104W51N], B. California, Nevada, Eastern Pacific Ocean, 10-km resolution, [128W31N x 113W44N]

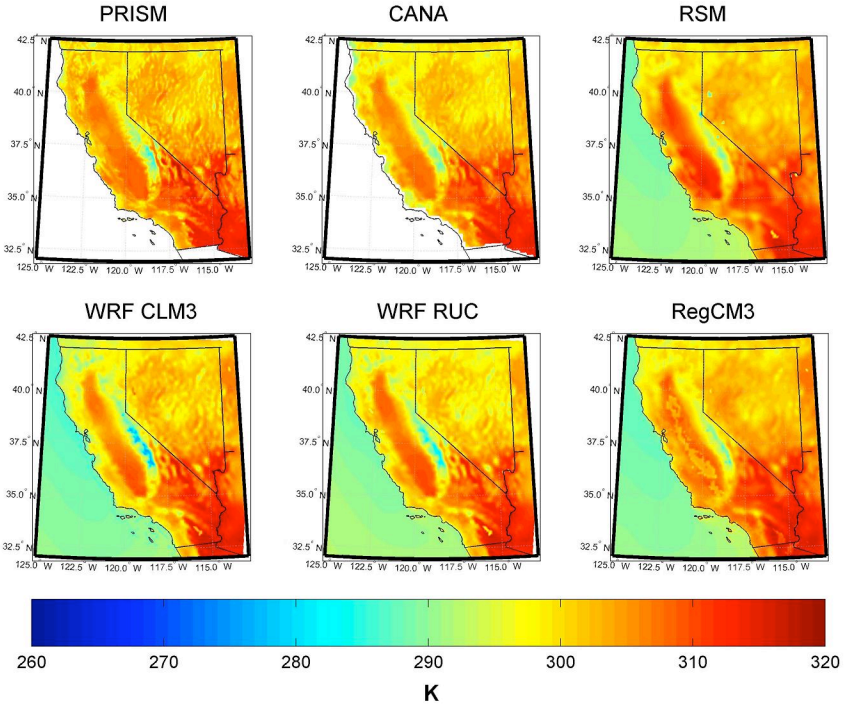

Figure 2a. Seasonal mean of daily maximum 2-m air temperature during June – August. Results shown are climatological means for 1980-1989.

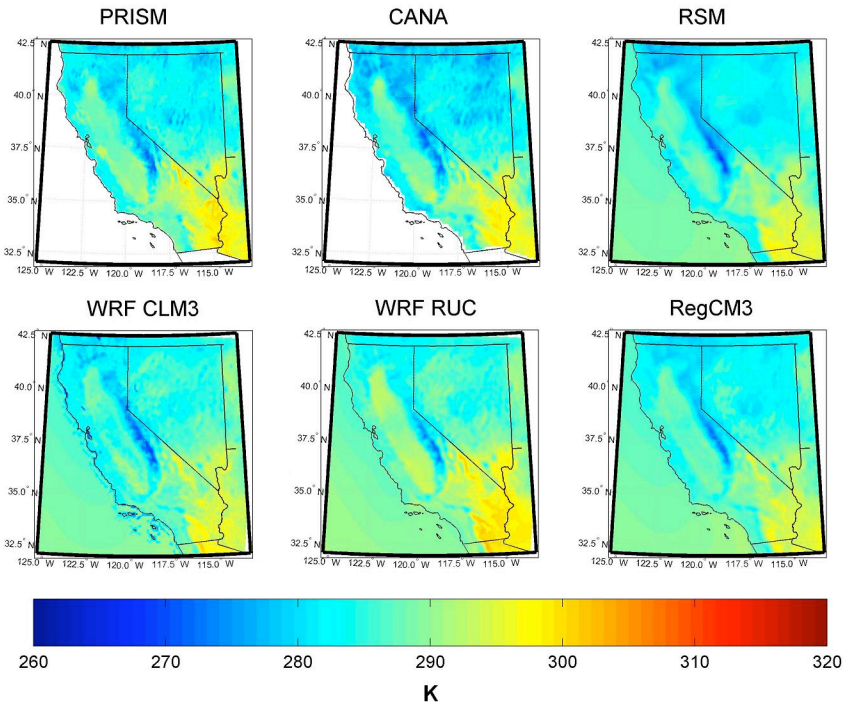

Figure 2b. Like Figure 2a, except for JJA daily minimum temperatures.

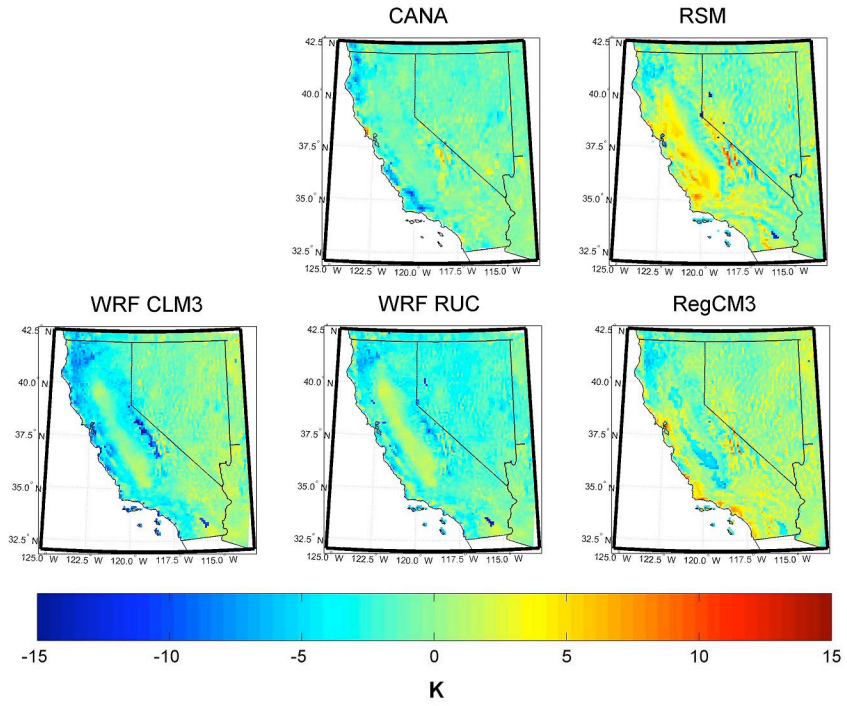

Figure 3A. Difference relative to PRISM in maximum 2-m air temperature during June – August.

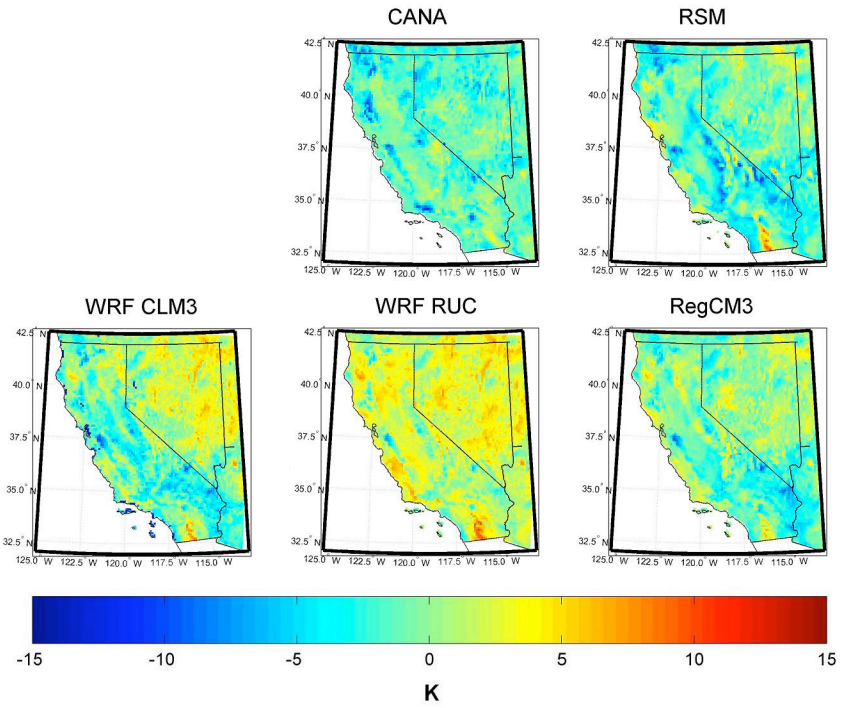

Figure 3B. Difference relative to PRISM in minimum 2-m air temperature during June-August.

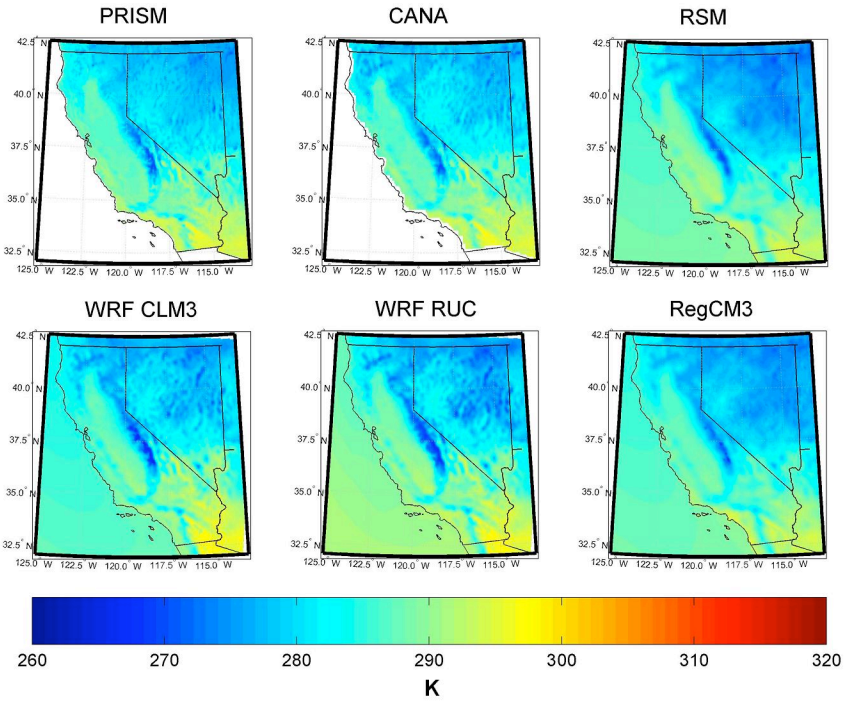

Figure 4A. Seasonal mean of daily maximum 2-m air temperature during December-February.

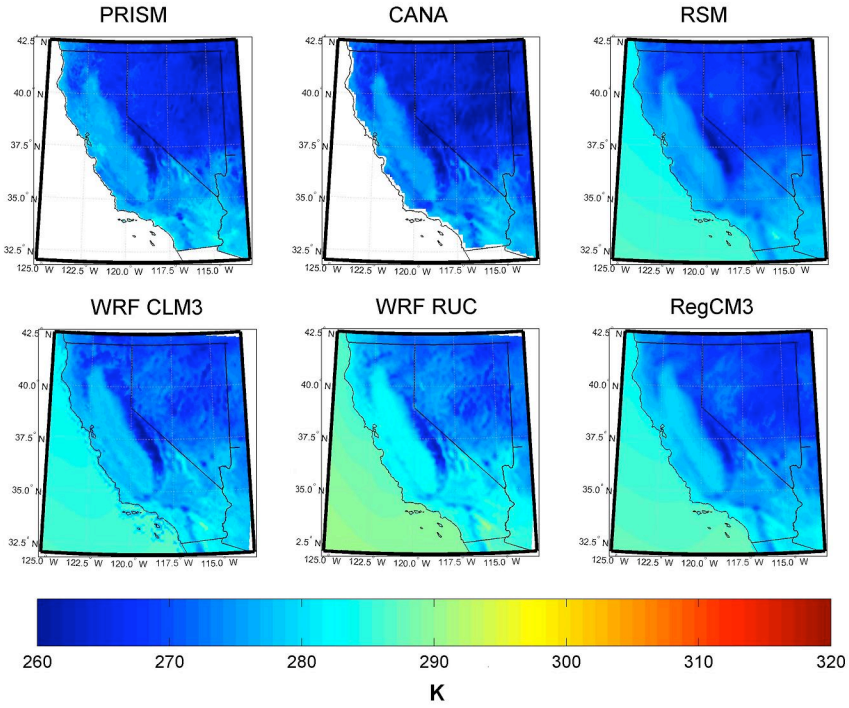

Figure 4B. Like Figure 4a except for DJF daily minimum temperatures.

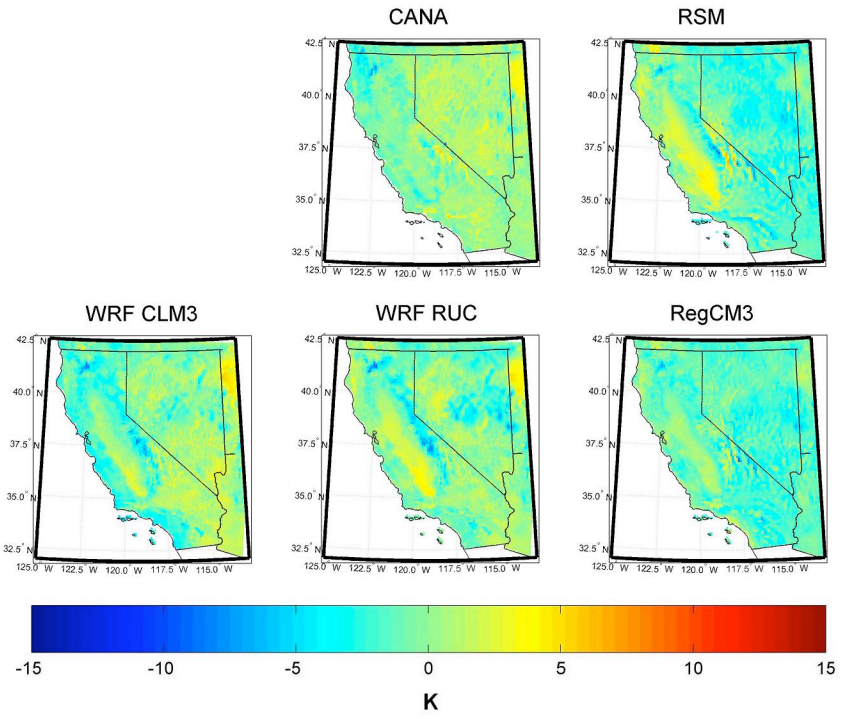

Figure 5A. Like Figure 3a except for December – February daily maximum temperatures.

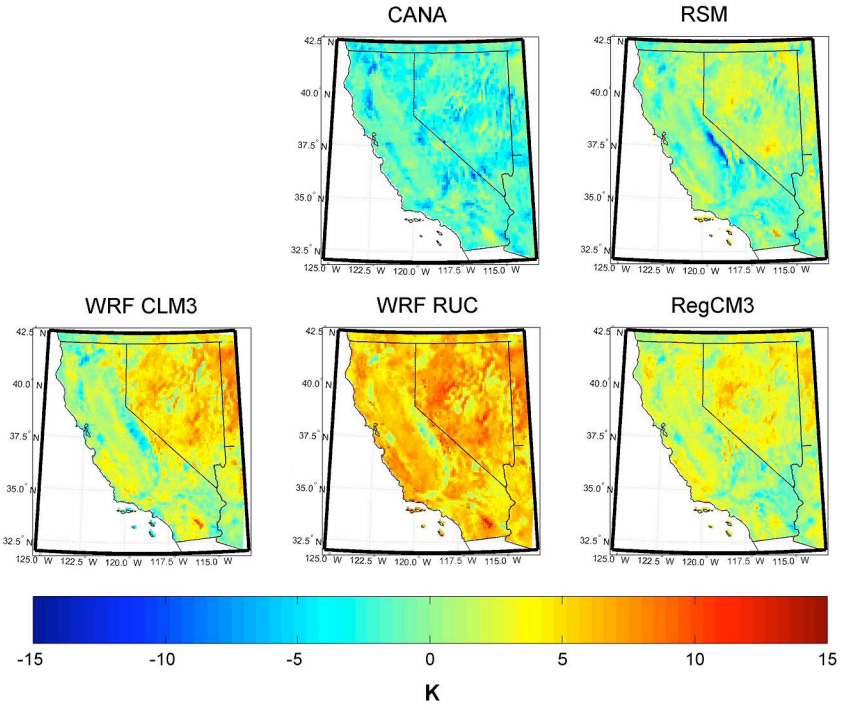

Figure 5B. Like Figure 5a except for DJF daily minimum temperatures.

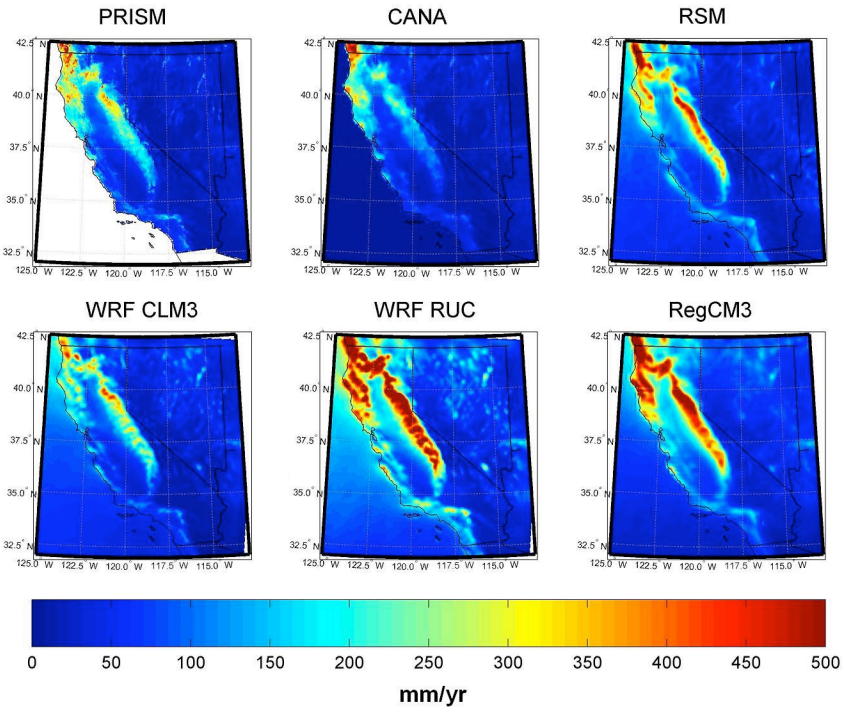

Figure 6A. Cumulative November-March precipitation, climatological mean for 1980-1989.

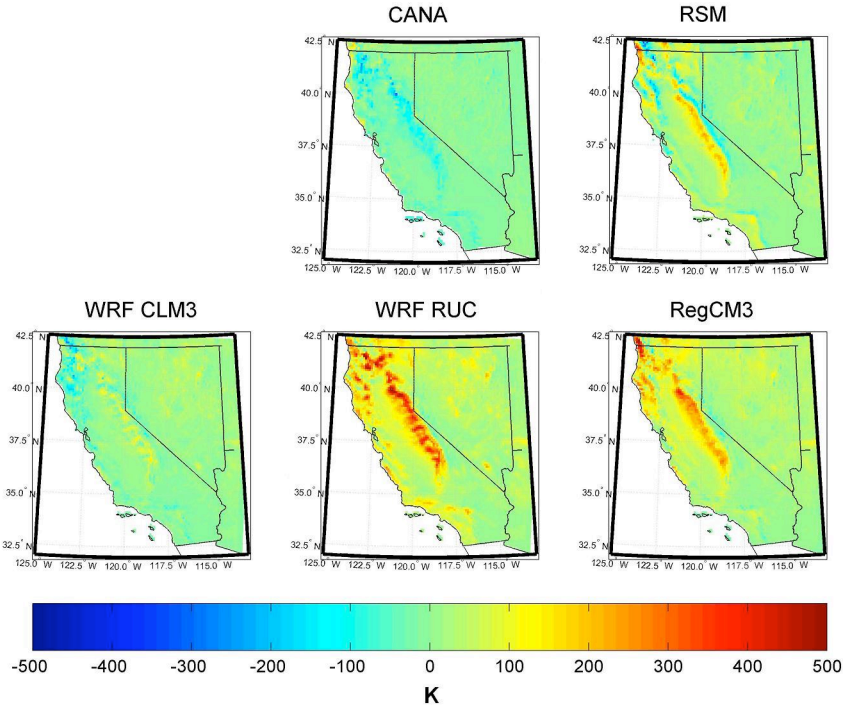

Figure 6B. Cumulative November – March precipitation differences relative to PRISM.

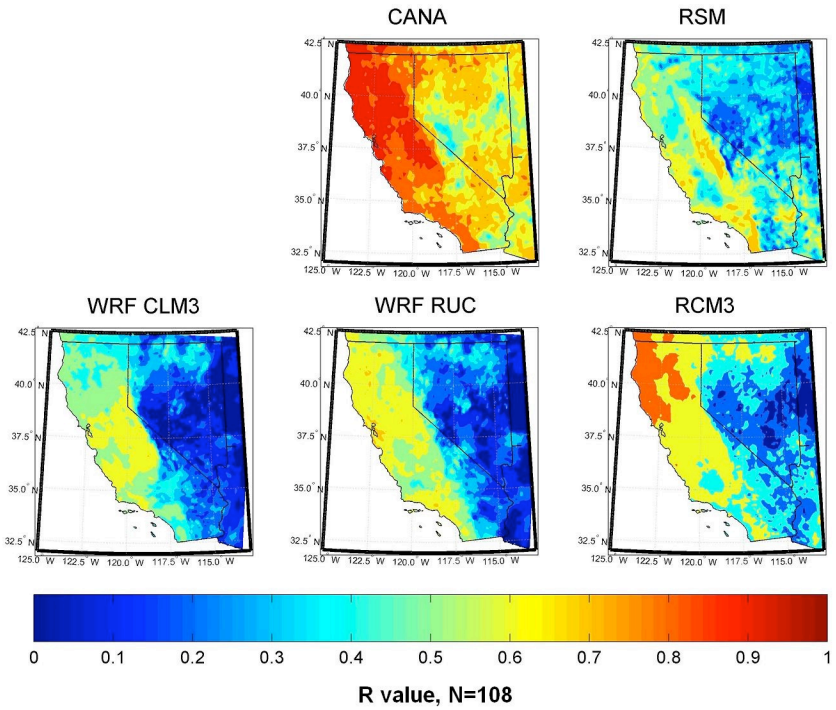

Figure 6C. Temporal correlations between monthly-mean precipitation in models and the PRISM observation-based data set.

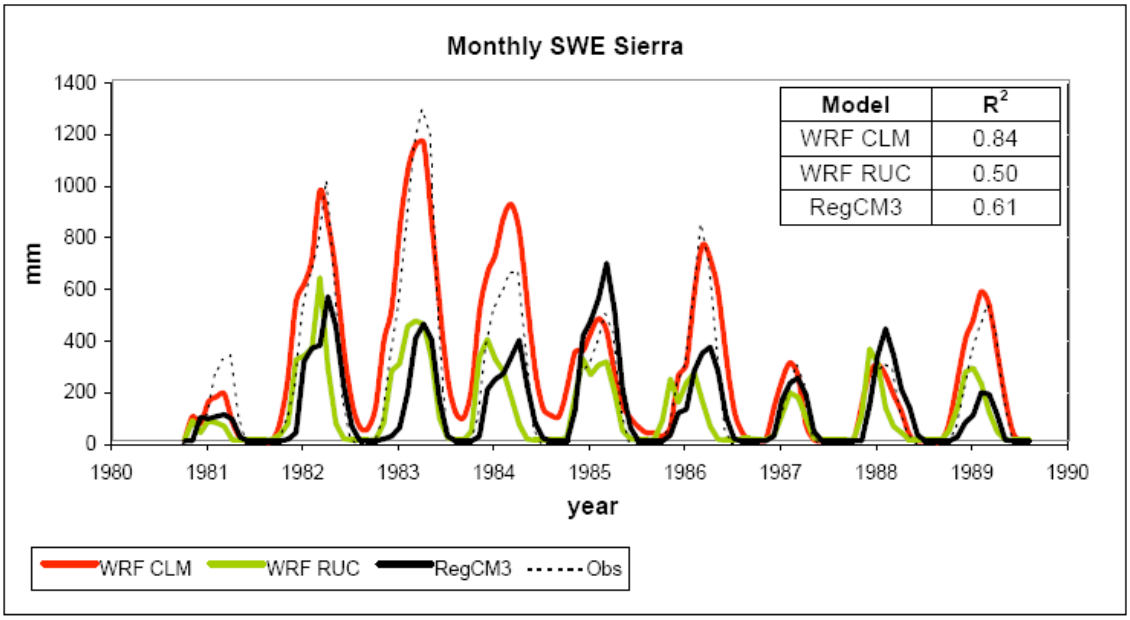

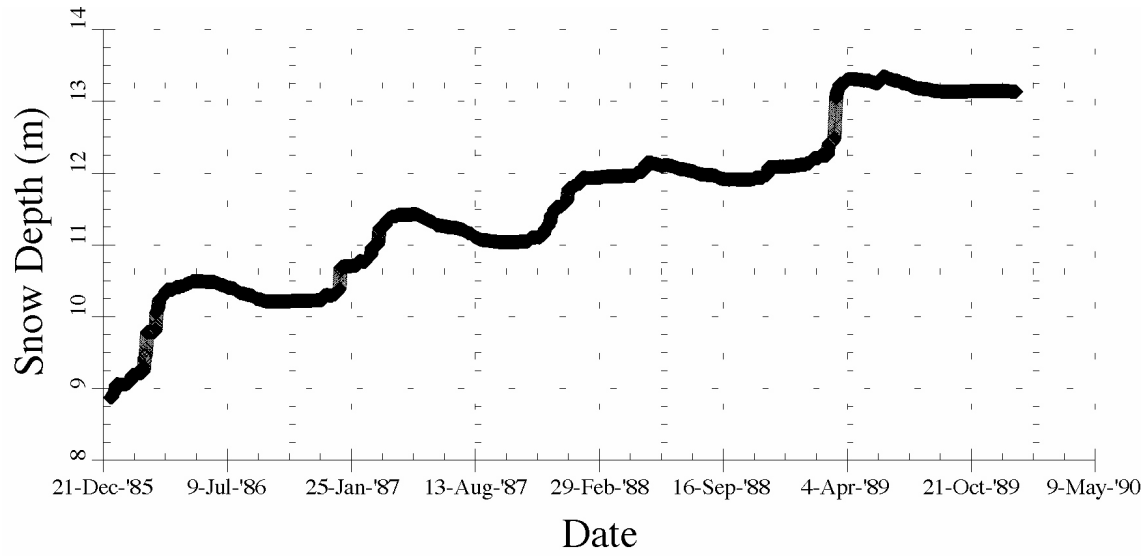

Figure 7. Top: Spatial mean Snow Water Equivalent (SWE) in a Sierra Nevada subdomain for WRF-CLM, WRF-RUC, RegCM3 with COOP observations. Bottom: Simulated SWE in one high-elevation grid cell in RegCM3.

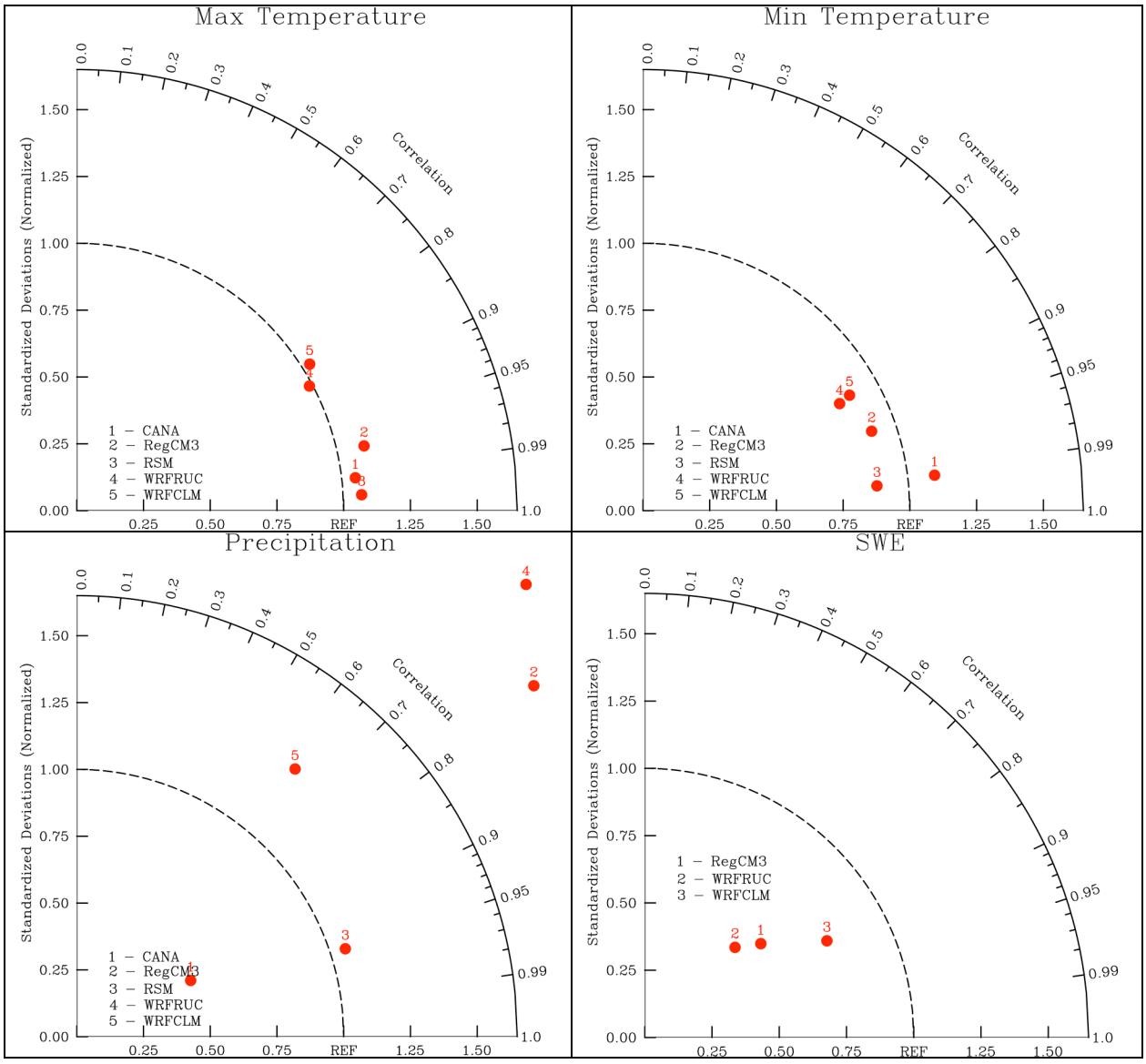

Figure 8. Taylor diagrams showing WRF-CLM, WRF-RUC, RSM, and RegCM model-to-observation performance scores based on normalized standard deviations and correlations for monthly means of (a) maximum temperature, (b) minimum temperature, (c) precipitation, and (d) SWE.

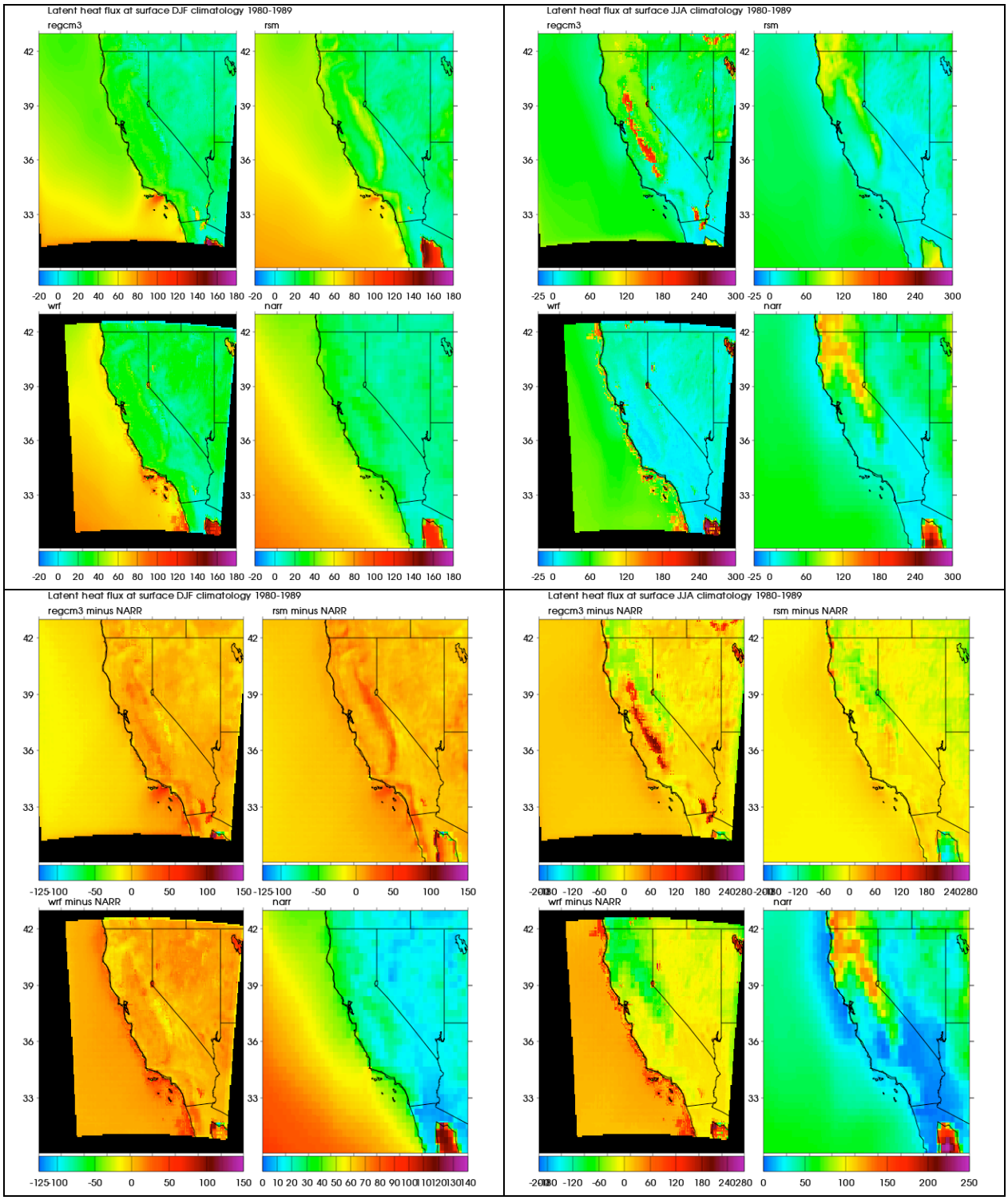

Figure 9: Surface latent heat fluxes. All results are climatological means for 1980-1989, for DJF (left two columns) and JJA (right two columns). Within each quadrant, the 4 panels show results from Regcm3, RSM, WRF-CLM, and the North American Regional Reanalysis (NARR). Top two rows show seasonal means from models and NARR; bottom two rows show differences between the models and NARR (i.e. model biases).

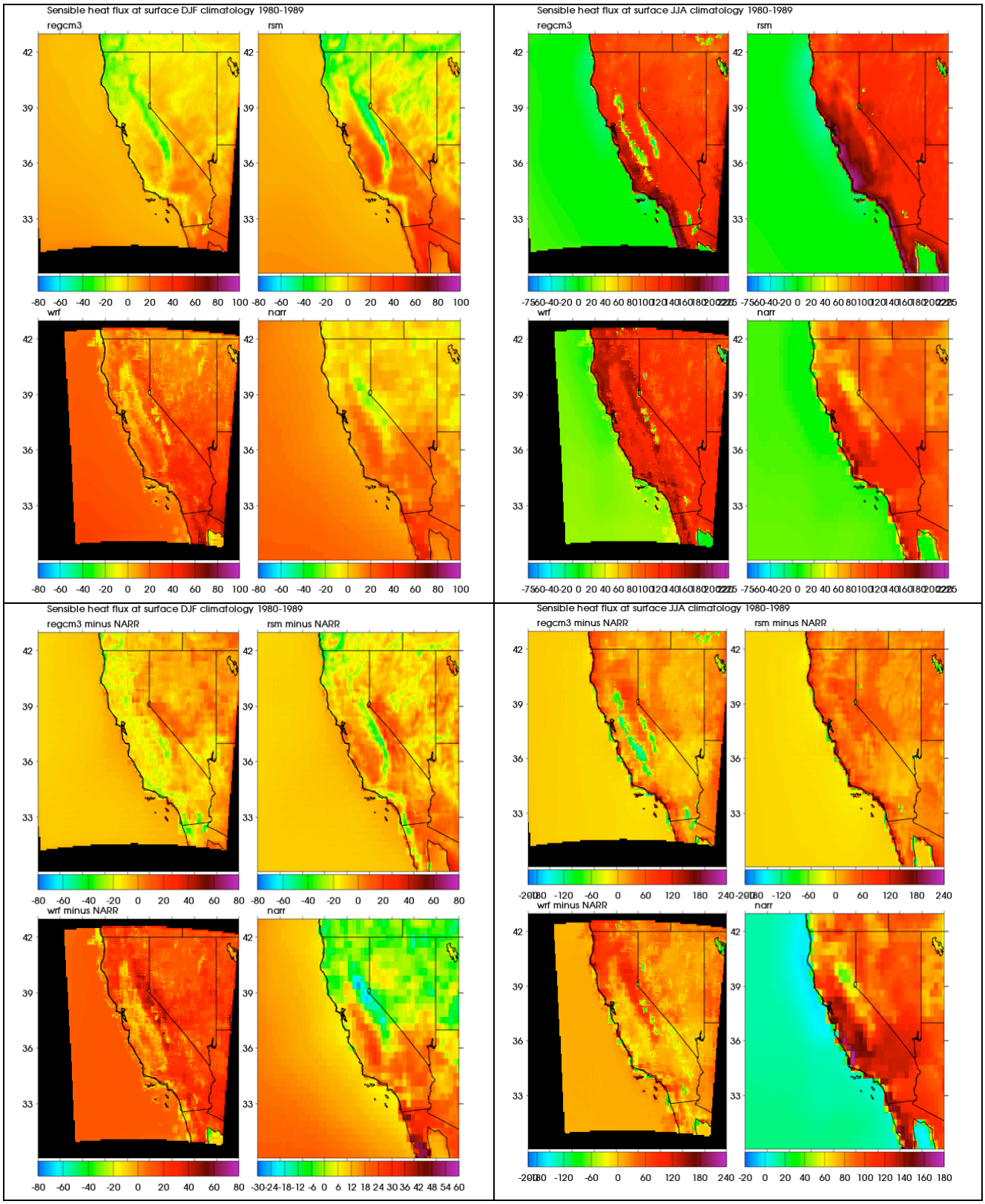

Figure 10: Same as Figure 9, except showing sensible hear flux at the surface.

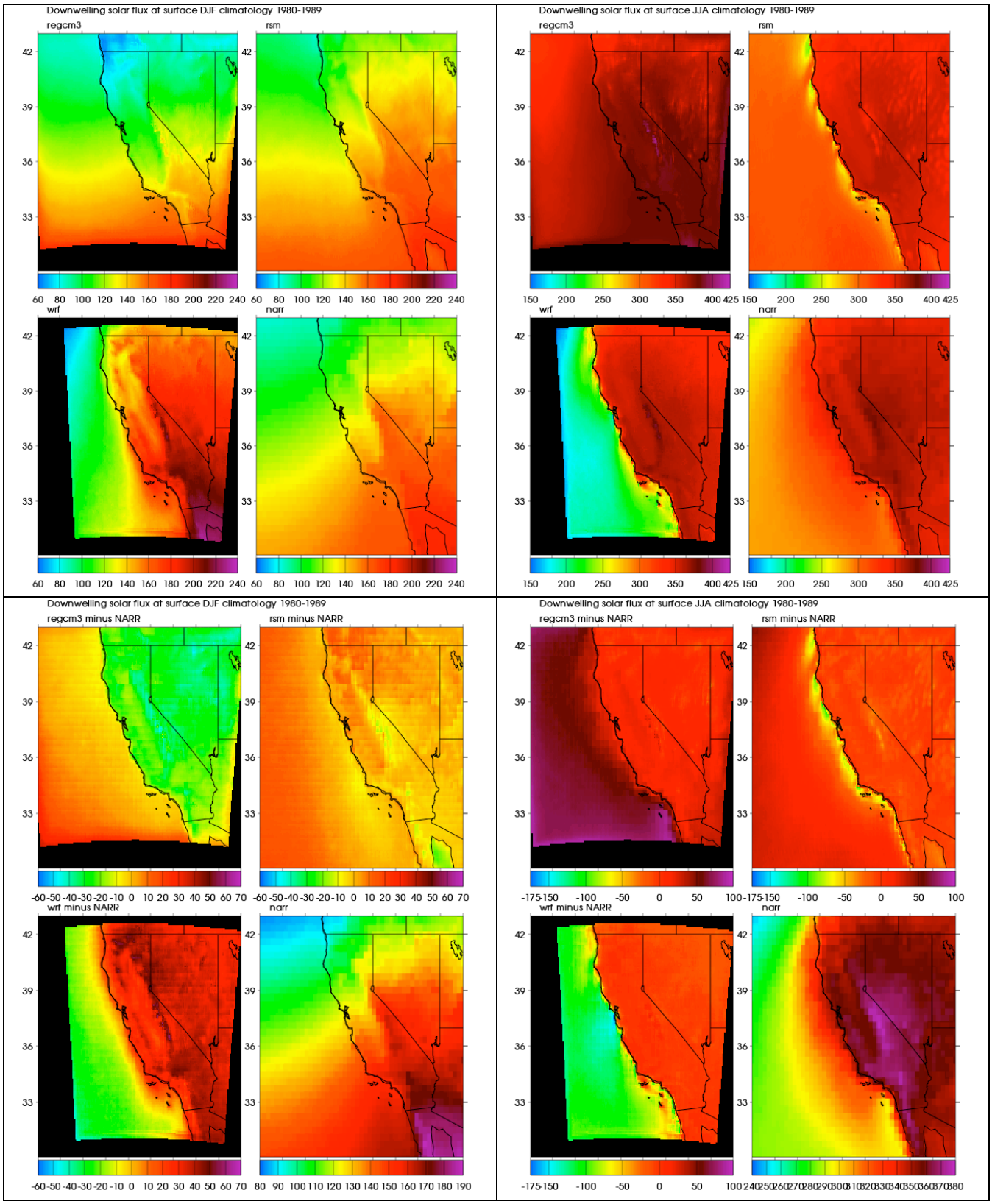

Figure 11: Same as Figure 9, except showing downwelling solar radiation at the surface.

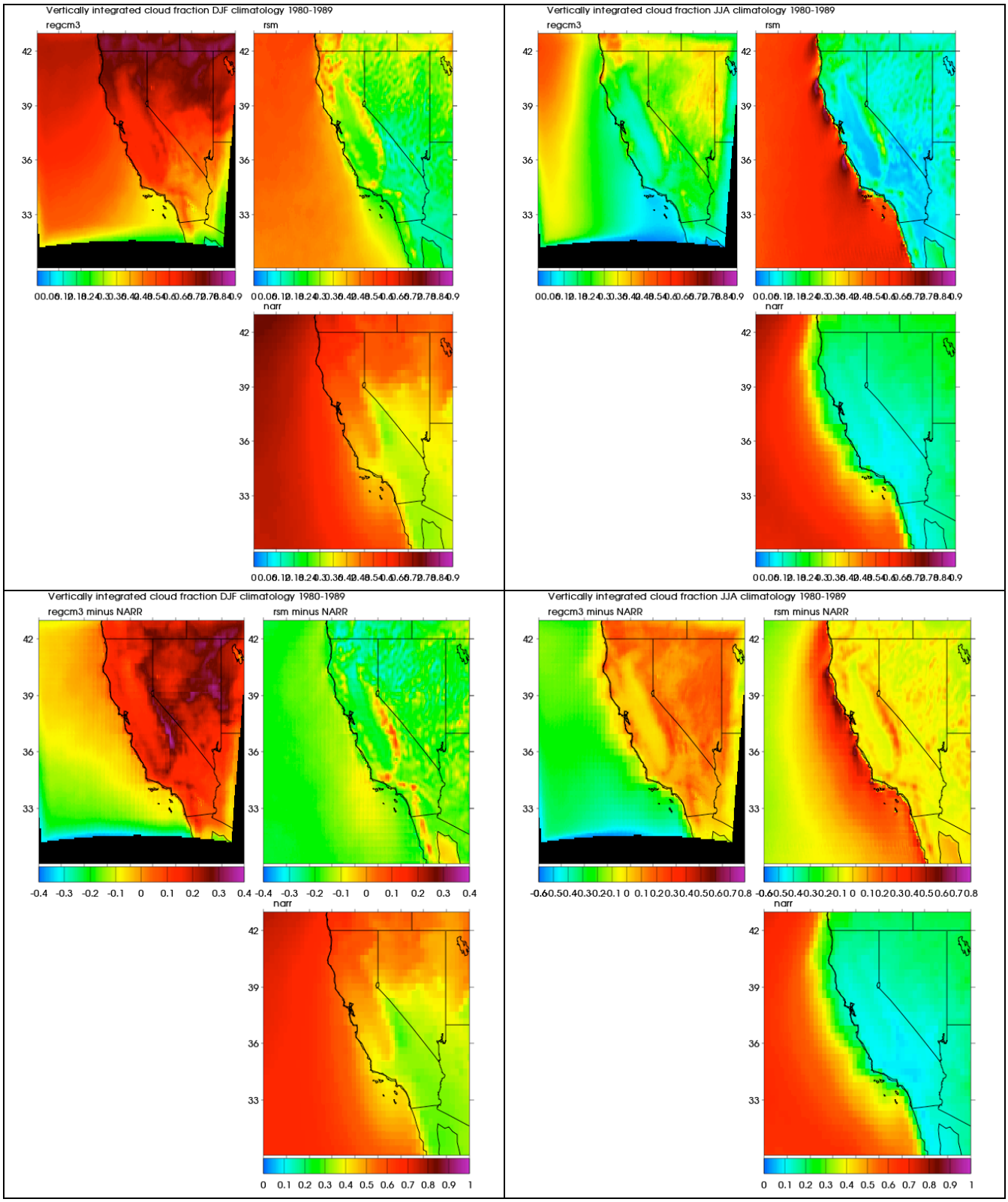

Figure 12: Same as Figure 9, except showing vertically integrated cloud fraction. Results from WRF-CLM are not available.

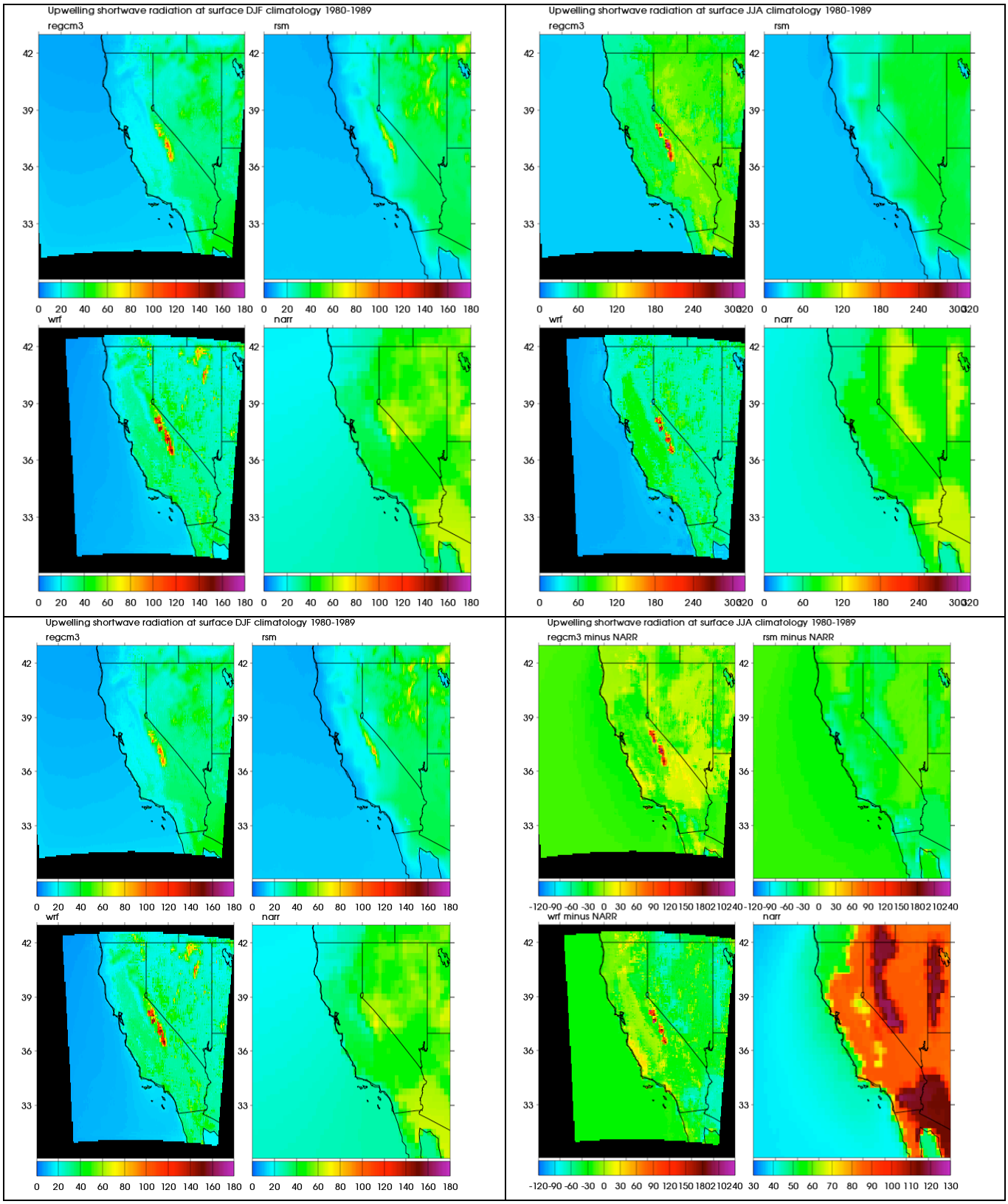

Figure 13: Same as Figure 9, except showing upwelling solar radiation at the surface.

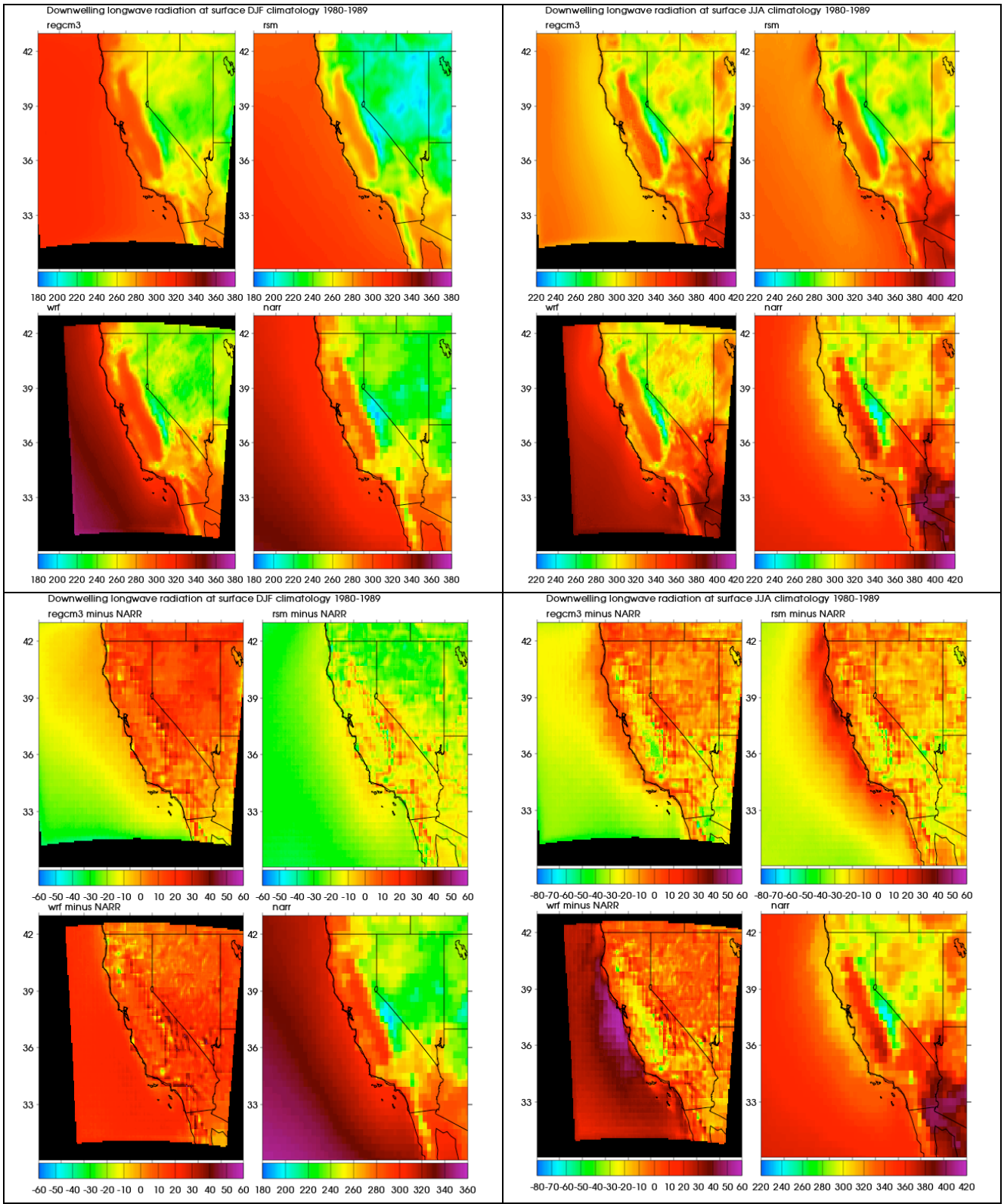

Figure 14: Same as Figure 9, except showing downwelling longwave radiation at the surface.

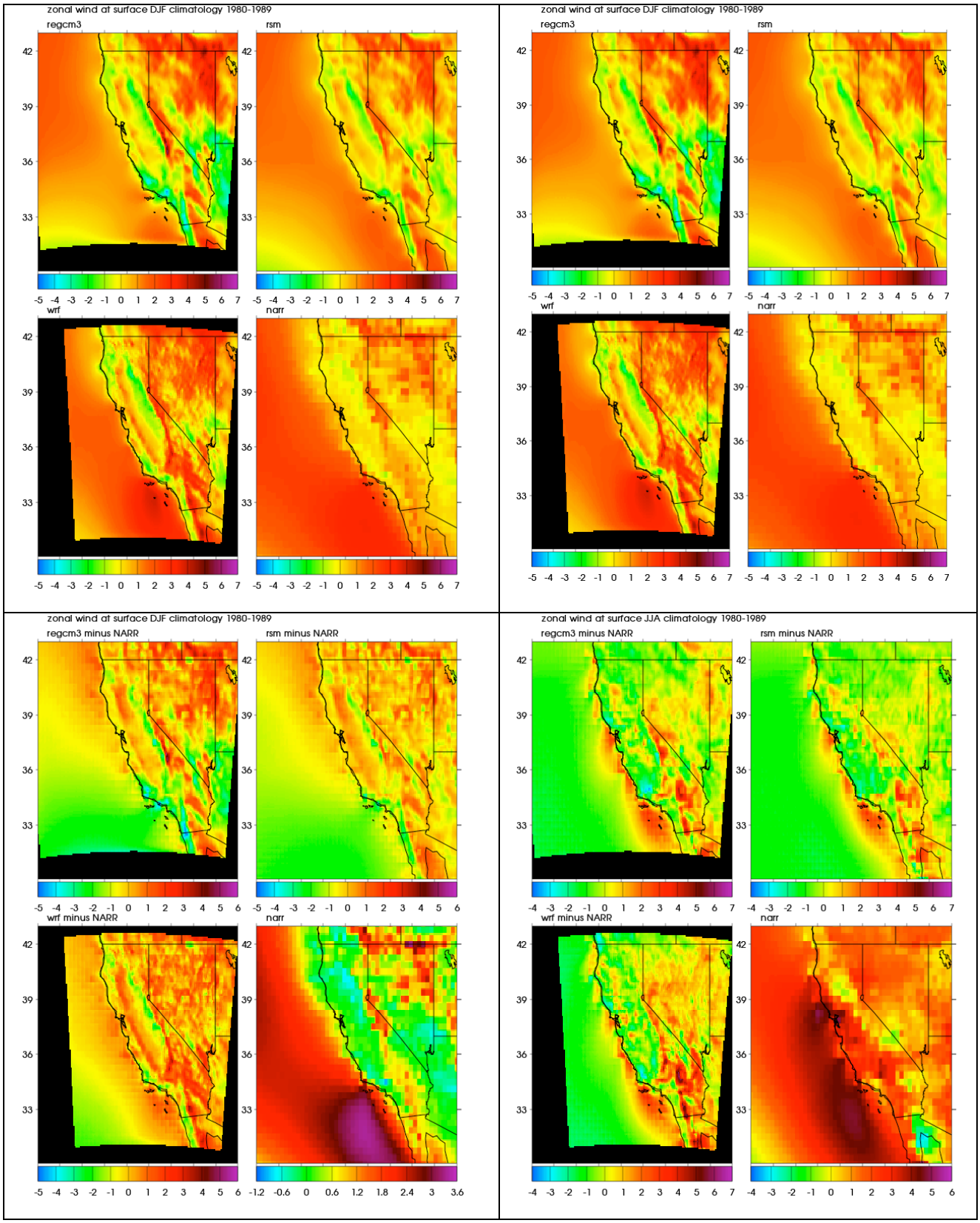

Figure 15: Same as Figure 9, except showing zonal wind component at the surface.

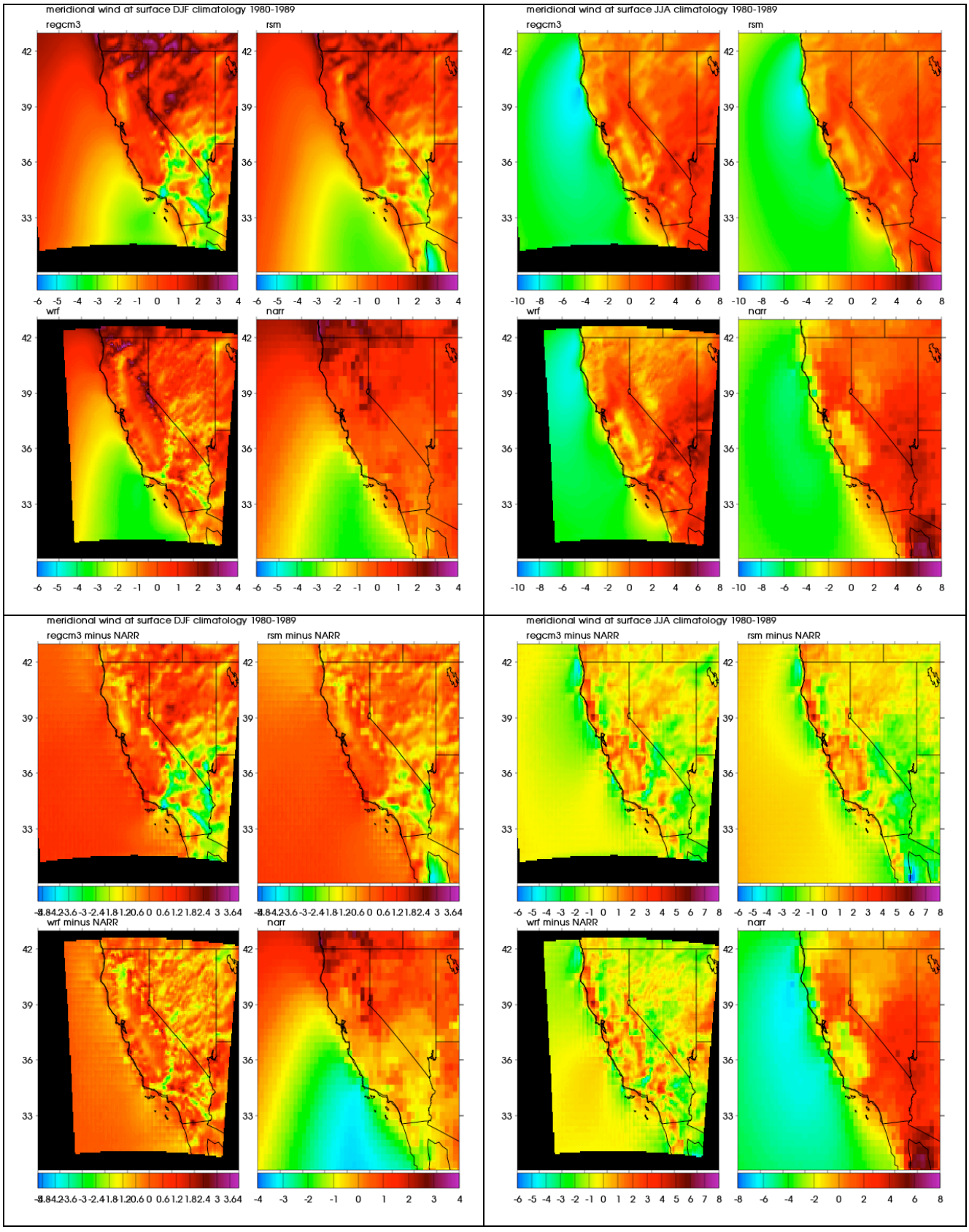
meridional wind at surface DJF climatology 1980-1989
regcm3
rsm
wrf
narr
meridional wind at surface JJA climatology 1980-1989
regcm3
rsm
wrf
narr
meridional wind at surface DJF climatology 1980-1989
regcm3 minus NARR
rsm minus NARR
wrf minus NARR
narr
meridional wind at surface JJA climatology 1980-1989
regcm3 minus NARR
rsm minus NARR
wrf minus NARR
narr

Figure 16: Same as Figure 9, except showing meridional wind component at the surface.

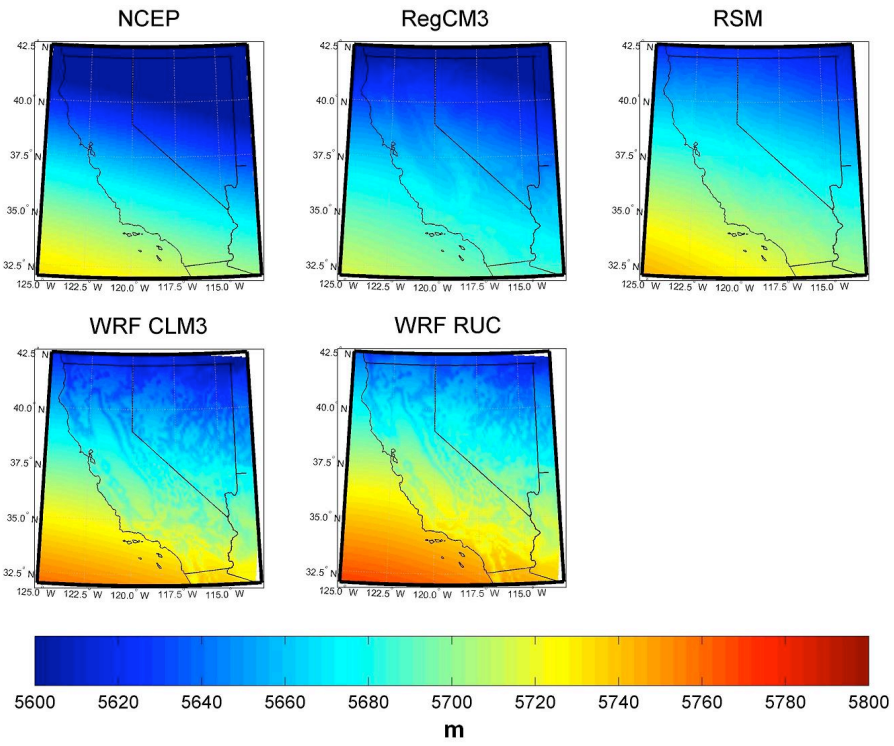

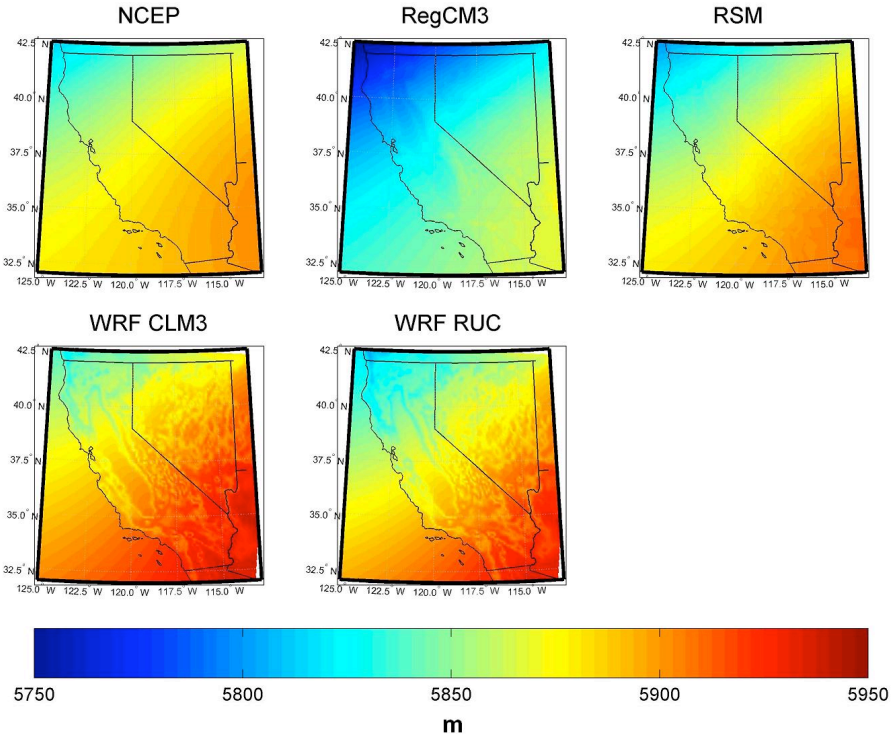

Figure 17. Geopotential Height (a) January mean-monthly distribution and (b) July mean-monthly distribution.

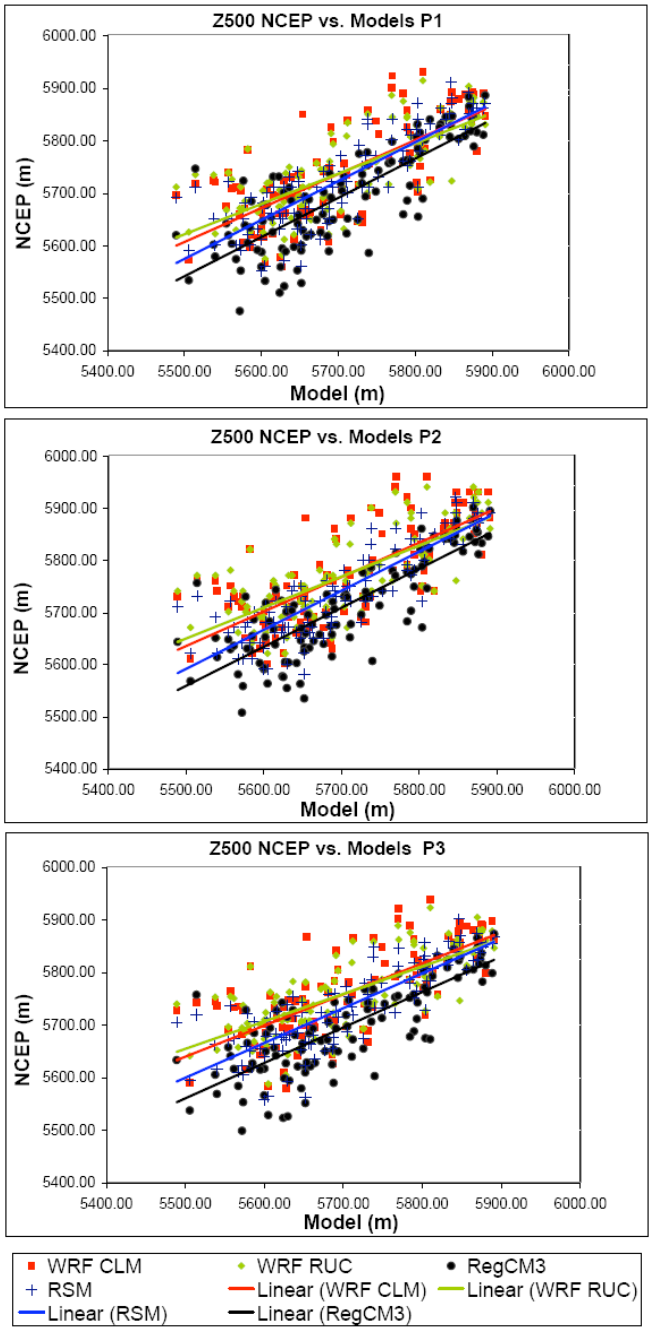

Figure 18. Model and Reanalysis comparison of the 500 hPa geopotential height for three locations P1. 120W, 39N (American River Basin), P2. 117.5W, 37N (Merced Basin), and P3. 122.5W, 38N (Russian River Basin).

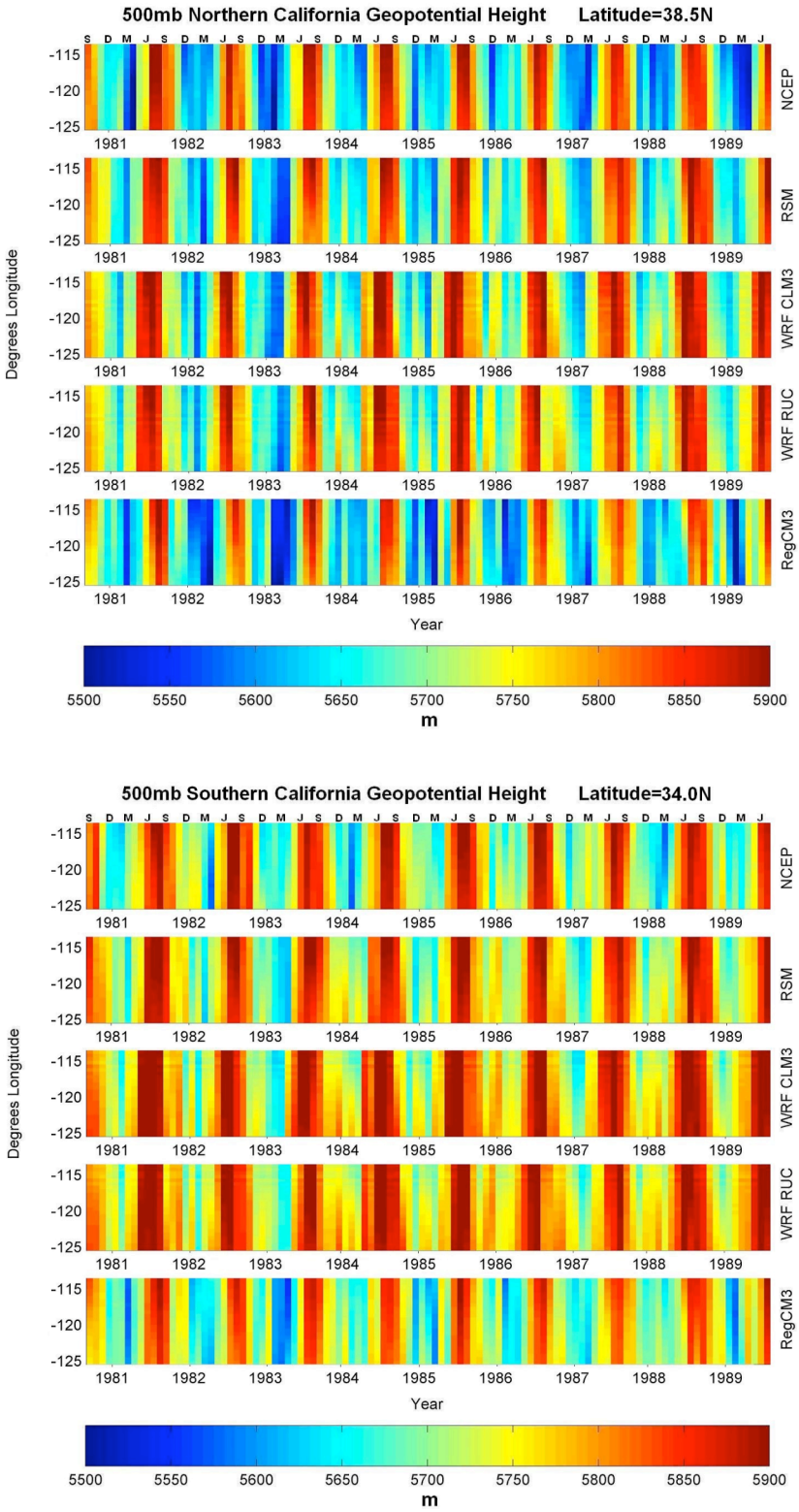

Figure 19. Hovmueller plots of the 500 hPa geopotential heights (a) 38.5N and (b) 34N.

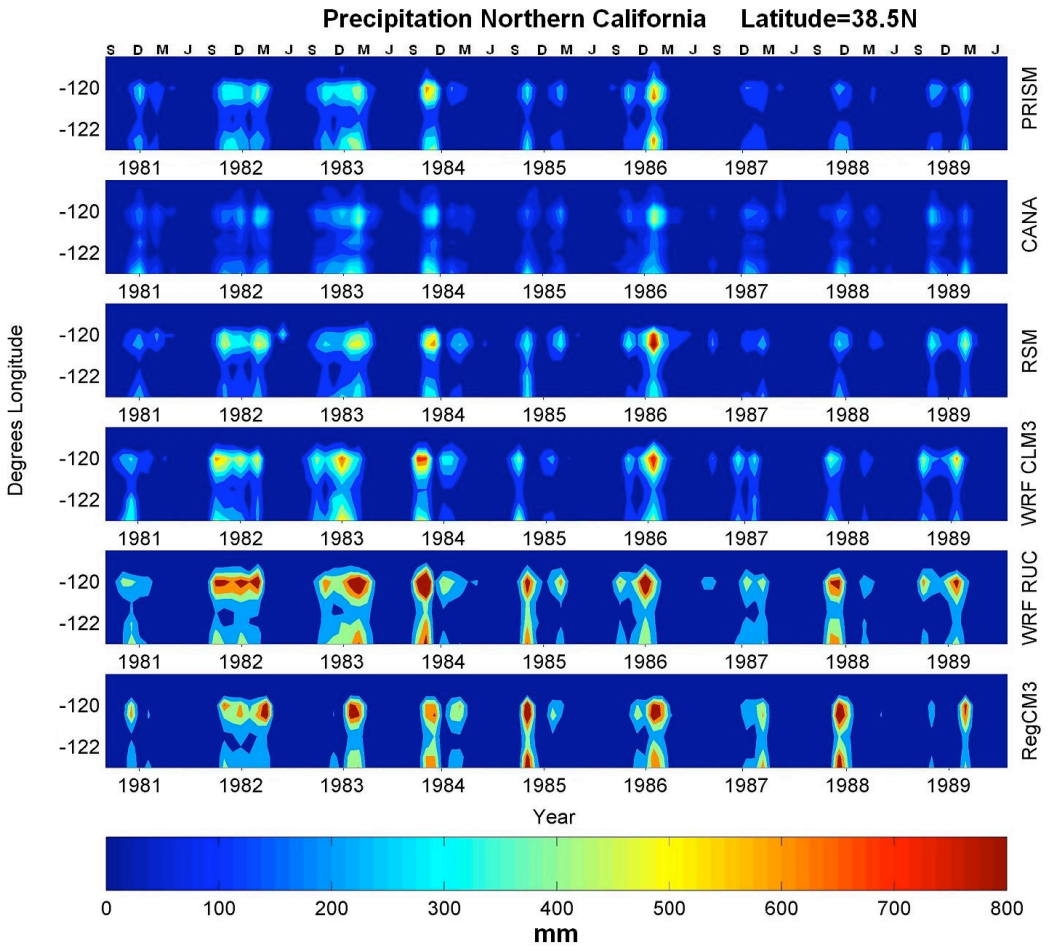

Figure 20. Hovmueller plots of the winter precipitation across latitude 38.5N .